Final Scientific/Technical Report

Date of Report: May 29, 2016

Award Number:	DE-FG36-05GO15049	
Project Title:	**Hot Rolling Scrap Reduction through Edge Cracking and Surface Defects Control**	
Recipient Organization:	University of Illinois at Urbana-Champaign 1206 W. Green St., MC-244 Urbana, IL 61801	
Partners:	Mark James Alcoa Technical Center	Mark.A.James@alcoa.com
Principal Investigator:	Armand J. Beaudoin	beaudoi@uiuc.eadu
Business Contact:	John K. Wierschem	jwiersch@illinois.edu
DOE Technology Manager:	Stephen Sikirica	Stephen.Sikirica@ee.doe.gov
DOE Project Officer:	Gibson Asuquo	Gibson.Asuquo@go.doe.gov
DOE Project Monitor:	McDaniel, Kristen	Kristen.McDaniel@ee.doe.gov
DOE Contract Specialist:	Scott Schmitz	Scott.Schmitz@go.doe.gov

Acknowledgement: “This material is based upon work supported by the Department of Energy under Award Number DE-FG36-05GO15049.”

3. Executive Summary

The design of future aircraft must address the combined demands for fuel efficiency, reduced emissions and lower operating costs. One contribution to these goals is weight savings through the development of new alloys and design techniques for airframe structures. This research contributes to the light-weighting through fabrication of monolithic components from advanced aluminum alloys by making a link between alloy processing history and in-service performance. Specifically, this research demonstrates the link between the turning, or deviation, of growing cracks with features of the alloy microstructure that follow from thermo-mechanical processing. This is achieved through a computer model of crack deviation. The model is validated against experimental data from production scale aluminum alloy plate, and demonstration of the effect of changes in processing history on crack deviation is made. The model is cast in the open-source finite element code WARP3D, which is freely downloadable and well documented.

This project provides benefit along several avenues. First, the technical contribution of the computer model offers the materials engineer a critical means of providing guidance both upstream, to process tuning to achieve optimal properties, and downstream, to enhance fault tolerance. Beyond the fuel savings and emissions reduction inherent in the light-weighting of aircraft structures, improved fault tolerance addresses demands for longer inspection intervals over baseline, and a lower life cycle cost.

4. Comparison of the Actual Accomplishments with the Goals and Objectives of the Project

4.1 Background, goals and objectives

The design of future aircraft must address the combined demands for fuel efficiency, reduced emissions and lower operating costs. Among requirements are significant weight savings, longer inspection intervals over baseline, and a lower life cycle cost. Light-weighting of aircraft is achieved through development of advanced structural alloys and allied design strategies. A current approach lies in the transition from multi-piece to monolithic components. An example is show in Figure 4.1 where a multi-piece spar is replaced by a monolithic spar.

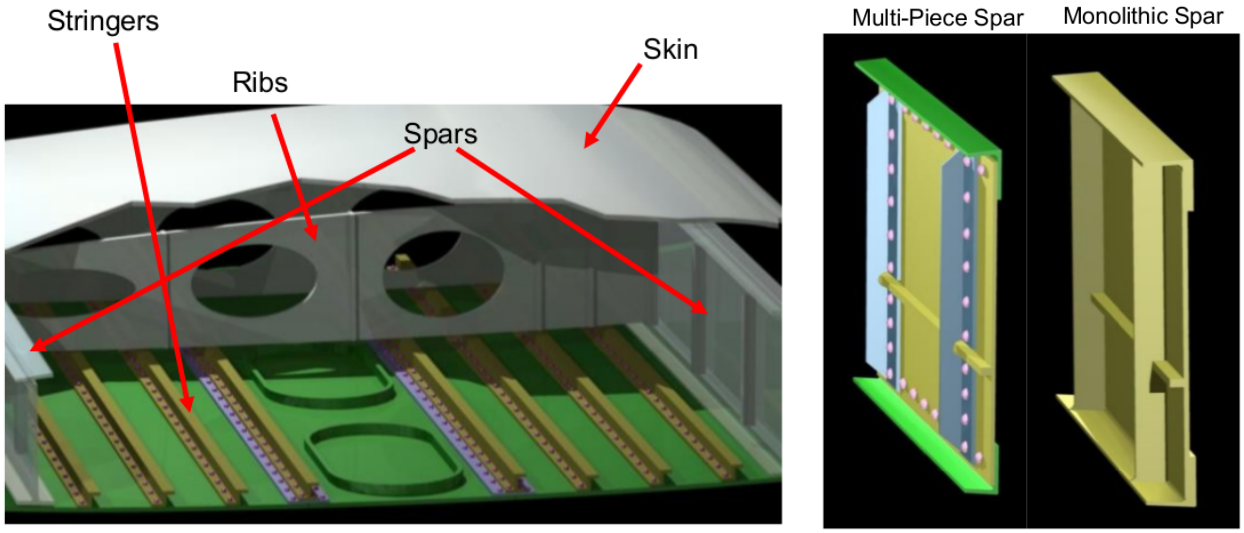

Figure 4.1 – Replace of a multi-piece spar with monolithic component: location of the spar in wing structure (left); comparison of multi-piece and monolithic spar (right). Figures courtesy of Dr. Mark James (Alcoa).

In the traditional design of a multi-piece structure, it is possible to exploit the properties of of the individual components as inherited from the processing history. For example, an extrusion specifically designed and processed to support bending loads may be oriented so as to sustain that particular state of loading. The change to monolithic construction brings about new opportunities, but also new challenges. Broadly speaking, rolled aluminum aerospace alloy products have quite directional properties, with properties in the short transverse (S) properties – those along the plate thickness – have lower strength relative to the rolling (L) and plate width (T) directions. At the scale of the plate microstructure, grains have a 'flattened' aspect that are thin in the (S) direction. In a monolithic component, the state of stress may be quite complex, leading to a complex interaction between a crack and the short transverse microstructure. Examples are shown in Figure 4.2.

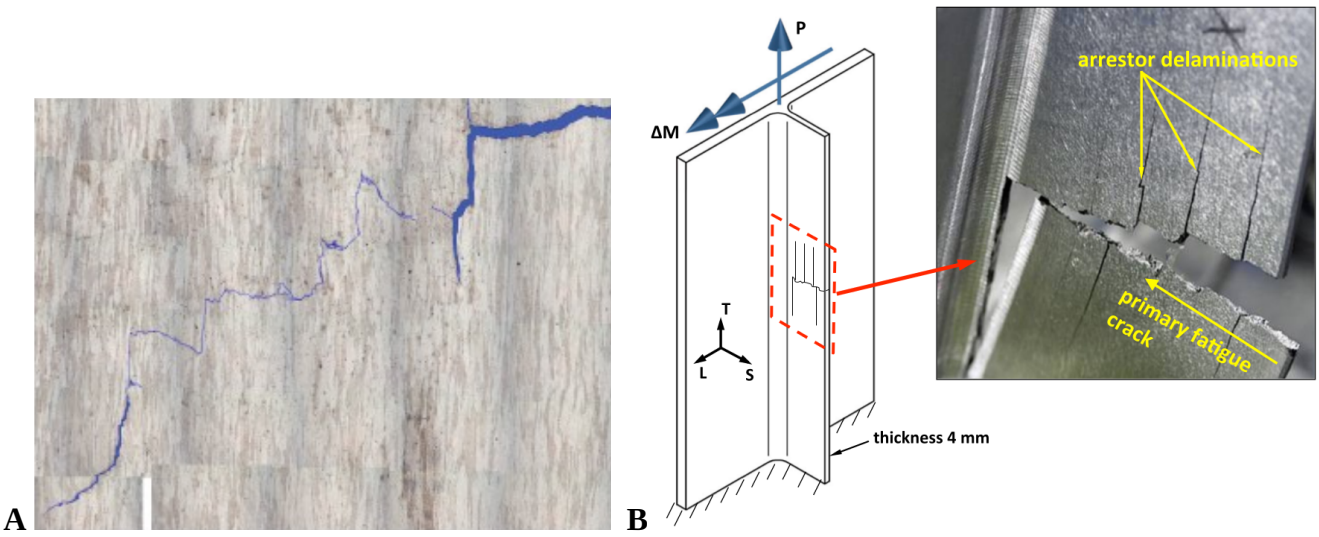

Figure 4.2 – Delaminations developed as a consequence of short transverse properties. A) a primary crack in a C(T) fracture specimen turns to follow grain boundaries which are extended in the vertical direction. B) Delaminations developed as a consequence of short transverse properties (S) in fatigue loading of an integrally-stiffened component, fabricated from an Al-Li alloys. Image courtesy of Lockheed-Martin and reproduced from Messner, Beaudoin & Dodds, Int. J. Fracture, 2014.

The scope of this project lies in the coding and implementation of a model for crack propagation in rolled aluminum plate, with tuning and validation following from a closely aligned experimental program. The overarching **goal** is a predictive capability that provides the connection between processing and product performance, relating crack propagation to processing history. As a further objective, the model must be readily applied using computational resources available in the industrial setting.

4.2 *Accomplishment: Prediction of crack turning in aluminum alloy plate*

The Key Milestone of the project is to *Accurately relate trends in crack growth in finished product with prior hot rolling practice*. The metric for success is to *Validate the model through prediction the stress intensity factor at the onset of crack branching in hard alloys within 20%*.

A suite of simulations were performed to achieve a parametric study for varying anisotropy (directionality in properties), yield strength and work hardening – with validation following from a coordinated experimental program. The experimental matrix follows. The experimental conditions are indicated by a pair of indices **(anisotropy, temper)**, where the anisotropy (directionality of properties) is related to the gauge thickness of the plate and the temper relates to the heat treatment. The experimental matrix is given in Table 4.1. Mechanical testing was performed for samples from the four experimental conditions. The characterization of work hardening and rate sensitivity (parameters necessary for the material model) is summarized in section 5. Samples for crack turning were prepared and tested at ATC.

Table 4.1 – Experimental Matrix

(1,1) • thin gauge • over-aged	**(1,2)** • thin gauge • peak-aged
(2,1) • thick gauge • over-aged	**(2,2)** • thick gauge • peak-aged

The degree of anisotropy for the two gauges was introduced through the selection of two distinct grain orientations, placed ahead of the crack tip, for the thin & thick gauge respectively (Figure 3a). These orientations were initially selected based on data collected from *in situ* studies performed at the Advanced Photon Source of Argonne National Laboratory. An outline of these supporting studies is given in Section 5. In brief summary, a pair of grains – one oriented favorably for slip on crystallographic planes and another less favorably – could develop marked differences in stress state. Because of the variation in plasticity between the two grains, associated with the 'effective stress', there is a concomitant mis-match in the 'hydrostatic stress' associated with volume change. It is the ratio of the hydrostatic stress to the effective stress that drives the evolution of damage. This is measured through the Rice-Tracey parameter, a function of this ratio, $\sigma_{eff}/\sigma_{mean}$.

The second index relates to the heat treatment condition and dictates the strength of the material. For each aging condition, yield stress and work hardening were entered into the model based on experimental measurements made at UIUC. In addition to the strength, a gradient term was included to provide for additional inhomogeneity in the plastic response at grain boundaries in the over-aged condition.

The mechanism leading to deviation, or turning, of the primary crack is shown in Figure 4.3. Two grains, labeled “1” and “2” share a vertical boundary perpendicular to the direction of crack growth (Figure 4.3a). These grains were selected from a pair of grains showing large mismatch in stress during *in situ* loading at the APS. *The damage (Rice-Tracey) parameter is evaluated as the maximum value developed on the boundary between grains 1 & 2.* A plot showing the evolution of the Rice-Tracey parameter with increasing loading, for simulations relating to each of the four experimental conditions, is shown in Figure 2. The critical value of the damage (Rice-Tracey) parameter for the onset of crack deviation was taken as 0.7. This provides simulation values for loading in ksi√in to compare with experiment, as shown in Figure 4.4.

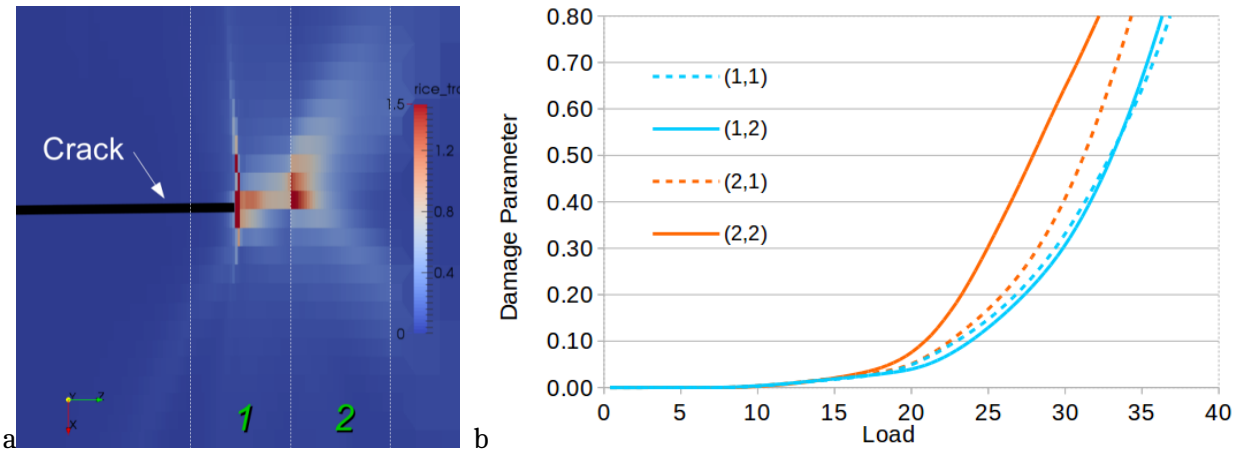

Figure 4.3 – a) contour plot of Rice-Tracey parameter. Evolution of the Rice-Tracey parameter with applied load.

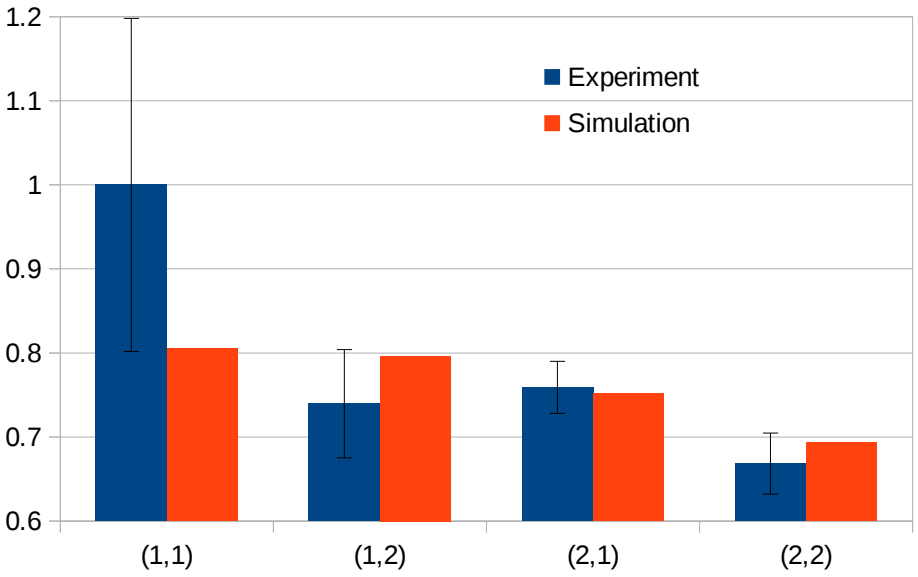

Figure 4.4 – Loading value at critical threshold of the damage parameter, normalized to average value for condition (1,1)

In Figure 4.4, simulation predictions match within 20% of the experimental value for onset of crack turning. *This meets the metric set forth in the Project Management Plan.* Results are also within the experimental error. The largest difference is for the (1,1) element of the experimental matrix, where the prediction is 19.8% lower than the experimental average. However, as can be seen by the error bars in Figure 3, there is a large variation for this particular processing condition, (1,1). If a single (large) outlying value is excluded, the average experimental value for case (1,1) is 0.89 (retaining the original normalization).

From the standpoint of predictive capability, the capture of general trends is more important than any particular match between experiment and simulation. The model reproduces the trend that thin gauge plate has higher values for onset of turning than thick gauge. For the thick gauge plate, the model captures the trend that the over-aged condition has onset of crack turning at larger loading as compared to the peak-aged condition.

In the case of the thinner plate, the difference between the two aging conditions is not distinguished by the model – *for the particular orientations chosen to represent the anisotropy;* note the similarity of lines for cases (1,1) & (1,2) in Figure 2. Said another way, local variations in anisotropy dominate in the simulation for the thin plate. An area for future work would be to explore different orientations: indications that the dominance of crystallographic orientation over parameters relating to temper may be a reason for the large variation in measurements for experimental (over-aged) condition (1,1). Note also that the model prediction is within 3% of the minimum experimental value.

4.3 Prediction of Edge Cracking in Rolling of Aluminum Plate

An integrated model for the analysis of production rolling operations has been implemented. This model incorporates detailed mesoscale models of damage evolution into a practical computation procedure for application in a production facility. This model and supporting experimental work is described in Tasks 1-3 of the following section 5.

A key contribution of our research, which is *generally applicable to the mechanical failure of aluminum alloys in both production and service*, is in experimental work that relates the development of local hydrostatic stress (the stresses that promote the growth of internal damage) with grain-to-grain interactions at the mesoscale (Beaudoin *et al.,* 2012). These state-of-the-art experiments have been conducted at the Advanced Photon Source at Argonne National Laboratory. The resulting test and analysis procedure for metals of technological interest is of general utility to industry.

4.4 Relevance to the Integrated Computational Materials Engineering (ICME) initiative

Taken together, the components of the project contribute to the Integrated Computational Materials Engineering (ICME) initiative. Key information on material behavior is captured within computational tools and further validated through state-of-the-art experimental procedures. The work culminates in practical manufacturing process simulation.

5. Summary of Project Activities for the Entire Period of Funding

Tasks comprising the project are summarized below. Tasks 1, 2 & 3 relate to Budget Period 1 and the prediction of cracking *upstream*, in the rolling process. Tasks 4 & 5 were performed in Budget Period 2 and move the prediction of cracking *downstream*, with regard to crack turning in hard aluminum alloys used in airframe construction.

5.1 -Task 1 Microstructural Model Development for Deformation and Failure Analysis

Quantitative metallographic and microstructural characterization construction of accurate 2D and 3D images of the microstructure, incorporating important morphological and crystallographic descriptions for micro-mechanical analysis will be the main objective of this subtask. Metallographic studies with microscopy (optical, SEM, and TEM) and image analysis will be done for identification of microstructural parameters at critical regions of the deforming material. Tests will be interrupted periodically at different strain levels.

Constitutive Response of AA 2024. The aluminum alloy AA 2024 is widely used in aircraft construction. Hot rolled AA 2024 plate is first heat treated to develop an O temper. The procedure consists of a gradual heating from room temperature 20°C to 425°C over 4h, holding at 425°C for 130 min and gradual cooling back to room temperature at −30°C/h. Two types of mechanical tests were then carried out to detail the kinetics of plastic flow. The incremental step test is conducted to determine the flow stress at small total strain amplitudes, up to roughly 0.5%. A particular advantage of this procedure lies in the capability to obtain several sets of data from a single specimen, which in turn provides for efficient determination of the yield response over a range of temperatures and strain rates. The work-hardening response, as well as a cross-check of the yield response from the incremental step test, is obtained using routine compression testing. In addition, a literature review is performed with the objectives of validating and extending our data set. The incremental step test will be addressed in this report.

In the incremental step test, a cyclic waveform of strain is enforced (Figure 5.1**).** The gradual increase and decrease in cyclic strain range allows the material to return to approximately zero stress and strain – even though plastic deformation occurred, which in essence is the mechanical condition it had before performance of the test. This waveform cycle is referred to herein as a “block”, and blocks are repeated on a sample with different strain rate and temperature conditions. Since the strain amplitude is controlled such that it increases gradually until it reaches a designated value, and it decreases to zero, this test minimizes the accumulation of plastic residual strain and stress. Hence, multiple tests at various temperatures and strain rates can be performed. In most cases, four blocks are run, each having ten strain cycles, as shown in Figure 5.1. Cyclic stabilization is typically achieved on the second block; however, four blocks are run to verify the stabilization. The temperatures are increased by 100°C from −100°C to 495°C. The strain rates tested are 1%/s, 0.1%/s, 0.01%/s, and 0.001%/s. Due to the small strain range utilized in cyclic testing, the tests at different strain rates are thus conducted on what is arguably the same stable microstructure. All data were acquired at cyclic counts much smaller than failure, ensuring fatigue damage did not influence the deformation observed.

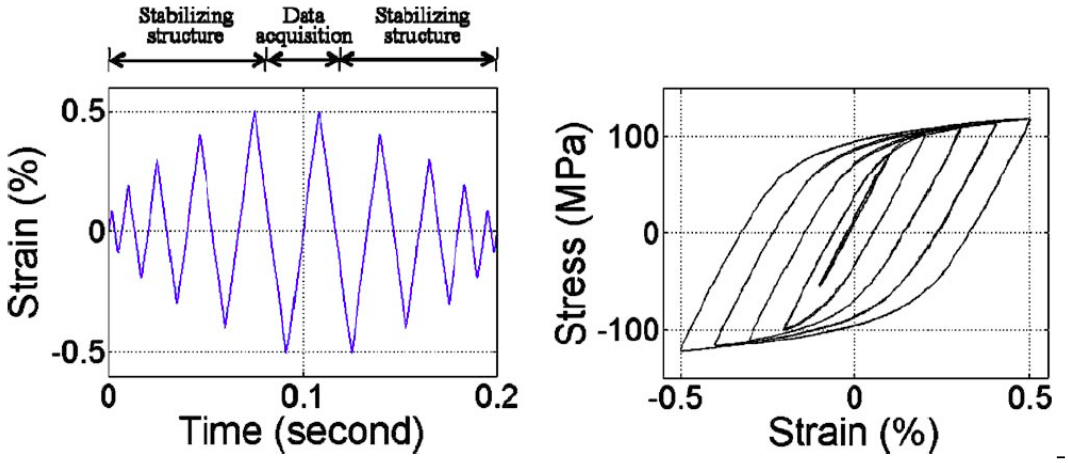

Figure 5.1: A 'packet' of data from the incremental step test.

The plot in Figure 5.2 summarizes the experimental test results as well as data from literature, as detailed in Kweon *et al*. (2009). The stress normalized by the shear modulus is plotted against a normalized energy of thermal activation,

$$g = \frac{kT}{\mu b^3}\ln\left(\frac{\dot{\varepsilon}_0}{\dot{\varepsilon}}\right)$$

There is qualitative agreement between the data developed using the incremental step test and this collective data set for yield stress derived from more traditional monotonic testing. Differences in the lower temperature/high strain rate regime are attributed to different definitions of the offset for yield. Since this material displays minimal strain hardening at higher temperatures, the offset definition does not impact these data. This is a result of considerable consequence: It supports the use of the incremental step test to explore the kinetics of yield. Considering the data $g^{\frac{1}{2}} > 0.5$, the collapse of yield data with data at moderate strains is indicative of a viscoplastic response with little or no work hardening. A linear scaling is evident between $g^{\frac{1}{2}}$ and the normalized measure of stress, $\left(\frac{\sigma}{\mu}\right)^{\frac{1}{2}}$. At values of $g^{\frac{1}{2}} < 0.5$, there is a noticeable transition in the response. The lower curve in this regime is obtained utilizing a 0.002 offset to define yield. The yield is rate-insensitive, indicative of a dynamic strain aging behavior. Data evaluated at a moderate level of total strain of roughly 0.1 indicate work hardening, the degree of which is marginally rate-sensitive.

The equations for the constitutive response following from this data are coded into material subroutines for application in the (macroscale) simulation of the rolling process. The equations and allied numerical procedure for use in finite element simulations are described in detail by Kweon (2009).

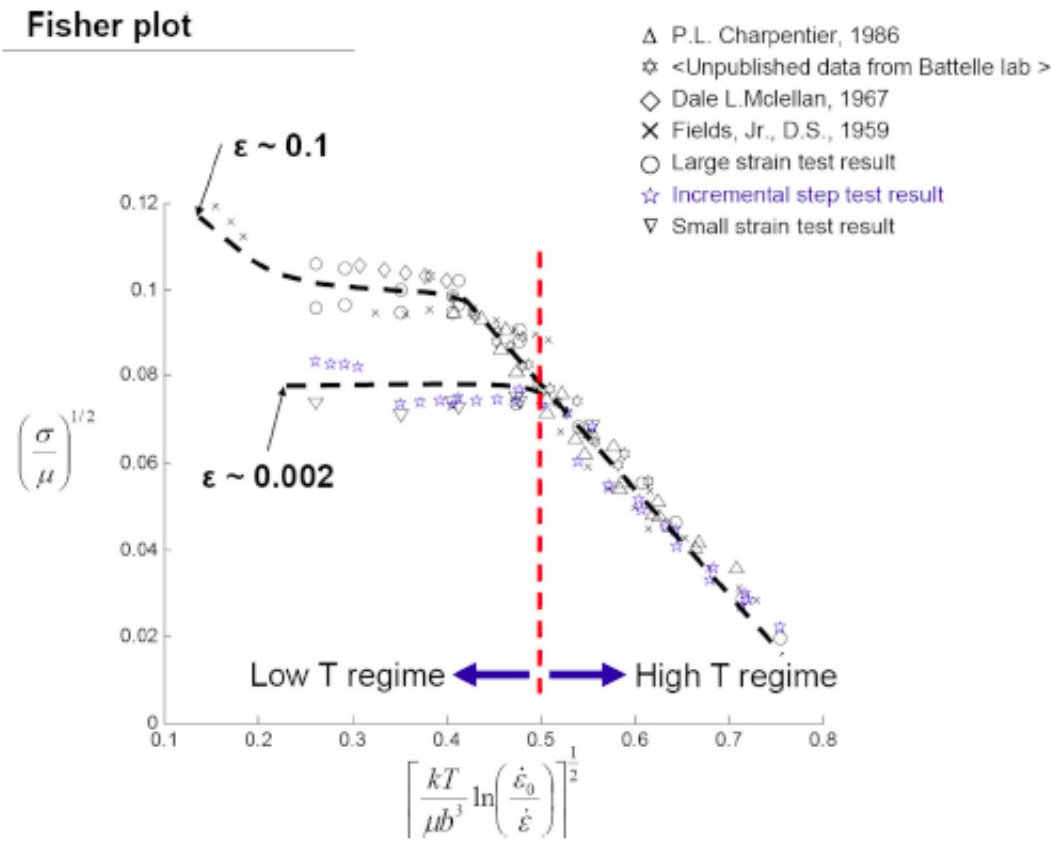

Figure 5.2: Plot of kinetics for plastic flow. Note the clear transition in response between 'hot' and 'warm' working.

Cracking with Varying Stress State An array of experimental tests has been performed, to span the combined state of hydrostatic and shear stress developed at the edge of rolled plate and slab. Stress conditions at the edge of rolled slab include a combine state of shear and normal stress. Several specimens have been designed to characterize the development of cracking in the presence of combined hydrostatic and shear stresses.

Specimen Design. A sample specimen (Figure 5.3, shown at right) mimics a similar design from Bao and Wierzbicki (2004). The gauge section is thinner than other areas to initiate shear deformation in a constrained region. Rate sensitive J_2 plasticity simulations, implemented with an ABAQUS UMAT, were done to choose optimal experimental settings. The constitutive equations and the solution techniques employed in the UMAT are detailed in the thesis by Kweon (2009).

Figure 5.3

Pin connection of the specimen to the load frame was made through the attachment grips to avoid any inhomogeneous deformation due to an initial misalignment, which can happen with other gripping scenarios, by accommodating specimen rotation making the gauge section align with the loading direction. The aluminum alloy used for the test is AA2024-O. The grain size is about 300 to 500 μm.

Digital Image Correlation (DIC). The specimens for DIC were carefully polished by hand using silicon carbide grinding papers, of grit sizes 320, 400, 600, 800. Once the surface was sufficiently free of flaws, black enamel paint was air-brushed onto the surface to make a random speckle pattern with speckle size about 5 μm. In order to obtain optimal results for DIC on a length-scale of 100 μm, an average speckle diameter of 5 μm was obtained by lightly spraying a mixture of 1-part flat black enamel paint and 3-parts paint thinner with an air-brush on the polished surface. Lighting and camera settings were adjusted such that the gray-scaled pixels spanned the 8-bit scale (256 is full-scale). Care was taken to ensure focus, lighting and surface/lens cleanliness during each experiment.

The experiments were conducted on a closed loop servo-hydraulic 100kN two-post load frame. System control and data acquisition were handled with a 32-bit closed-loop computer controlled system with a LabVIEW programming interface. Load was measured with a 100kN load cell while specimens were attached with a pin connection (Figure 5.4). 8-bit images with 1280 x 960 pixel resolution were recorded at 5fps (frame per second) while the deformation rate was applied at 0.1 mm/s.

Image correlation was obtained utilizing a commercial code, Vic-2D. A subset size of 35 pixels and a spacing of 5 pixels were employed to produce these results. Other subset sizes and spacings were examined, showing only small differences in all but extreme cases. The DIC correlation was performed using rigid body motion of the reference subset, and strains were post calculated as the gradient of the displacements. This procedure was required due to the large overall displacements of the specimen. A global threshold limit of 15 units was employed to eliminate propagating errors from small regions of poor correlation. The digital camera and lights are shown in Figure 5.4. Figure 5.5a shows the initial gauge section with random speckles, and the gauge section after fracture is provided in Figure 5.5b.

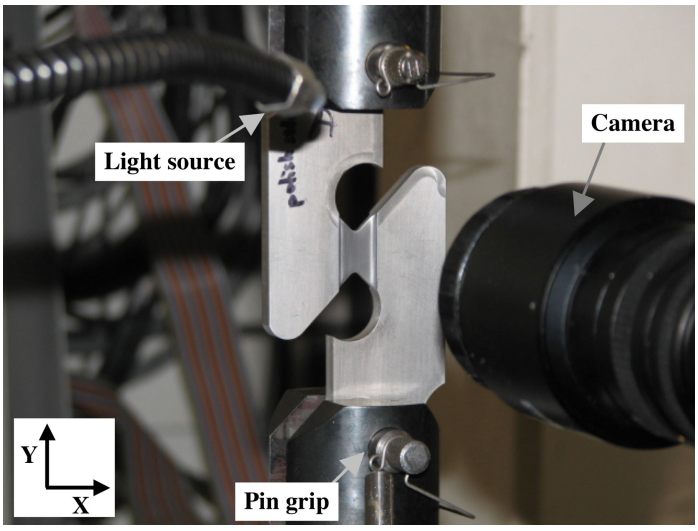

Figure 5.4: The test machine with a camera setup

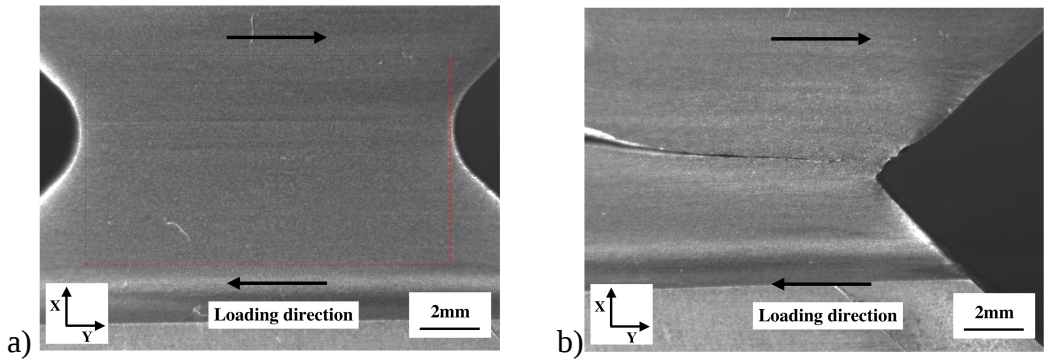

Figure 5.5: a) The initial gauge section with random speckles, the red dotted rectangle is the area of interest window for post correlation. b) The gauge section after fracture.

The pictures are rotated 90 degrees in Figure 5.5 as compared to the Figures 5.3 & 5.4 due to the camera setup position. The crack propagated slightly away from the centerline, where plastic deformation concentrates in a J_2 plasticity simulation.

Figure 5.6 shows the horizontal (horizontal in Figure 5.5, vertical in Figures 5.3 & 5.4) displacement measured by DIC at 0.4mm pin displacement. Figure 5.7 shows the shear strain ε_{xy} calculated by DIC at 0.4mm pin displacement.

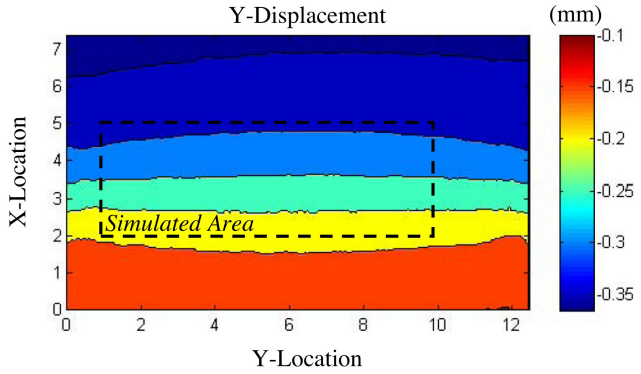

Figure 5.6: Horizontal displacements at 0.4mm pin displacement,
unit on the picture and the color bar: mm

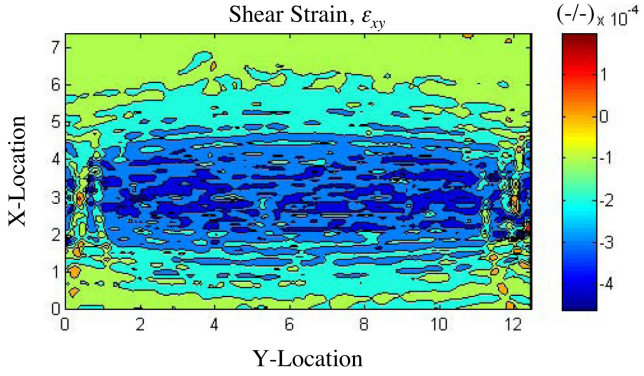

Figure 5.7: Shear strain at 0.4mm pin displacement,
unit on the picture: mm, unit in the scale bar: dimensionless

As shown in Figures 5.6 & 5.7, the displacement and shear strain ε_{xy} are not uniform along the horizontal direction. In case of ideal simple shear, the displacement and shear strain should be straight lines along the horizontal direction. Therefore, the non-linear contours in these Figures indicate that the deformation is not ideal simple shear: there is a gradient of shear strain along the horizontal direction. The shape of this contour also implies that there is some deformation component other than simple shear, which turns out to be a hydrostatic tension component.

Parametric Study of Shear in the Presence of Triaxiality. Samples were prepared from the aluminum alloy AA 2024 in the "O" temper condition, one of the materials under consideration in this project. The tests are denoted as "simple shear", "shear+tension", "shear+more-tension", "notched cylinder" (representative of several different notch sizes), and "thin plate with hole". Each test is paired with a finite element calculation. Whenever possible, a cross-check on the finite element result made using digitial image correlation (DIC). These specimens and allied finite element simulation results are shown in Figures 5.8-5.12. The key point to note is that the experiment provides the plastic strain at the onset of fracture in a variety of stress states.

It is the states of combined shear and tension that are of particular relevance to cracking at the edge of a plate, where lack of constraint relieves the hydrostatic component that contributes so fundamentally to rolling force and gradients in the transition from a state of plane strain to plane stress necessarily involve shear deformation.

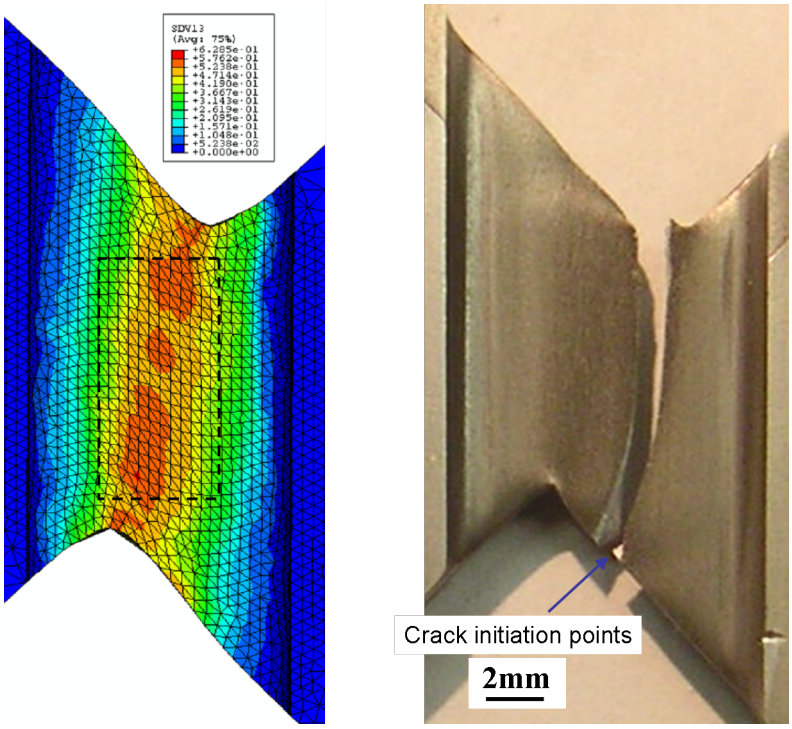

Figure 5.8: The simple shear specimen after fracture (right);
effective plastic strain, $\bar{\varepsilon}^{p}$ (left)

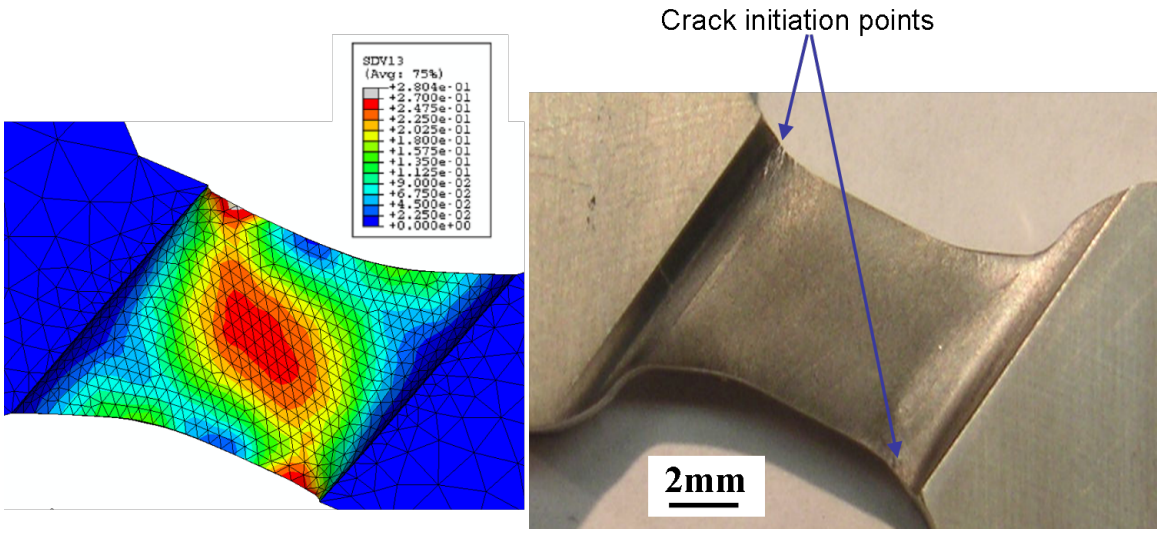

Figure 5.9: The shear+tension specimen at the onset of fracture (right); effective plastic strain, $\bar{\varepsilon}^p$ (left)

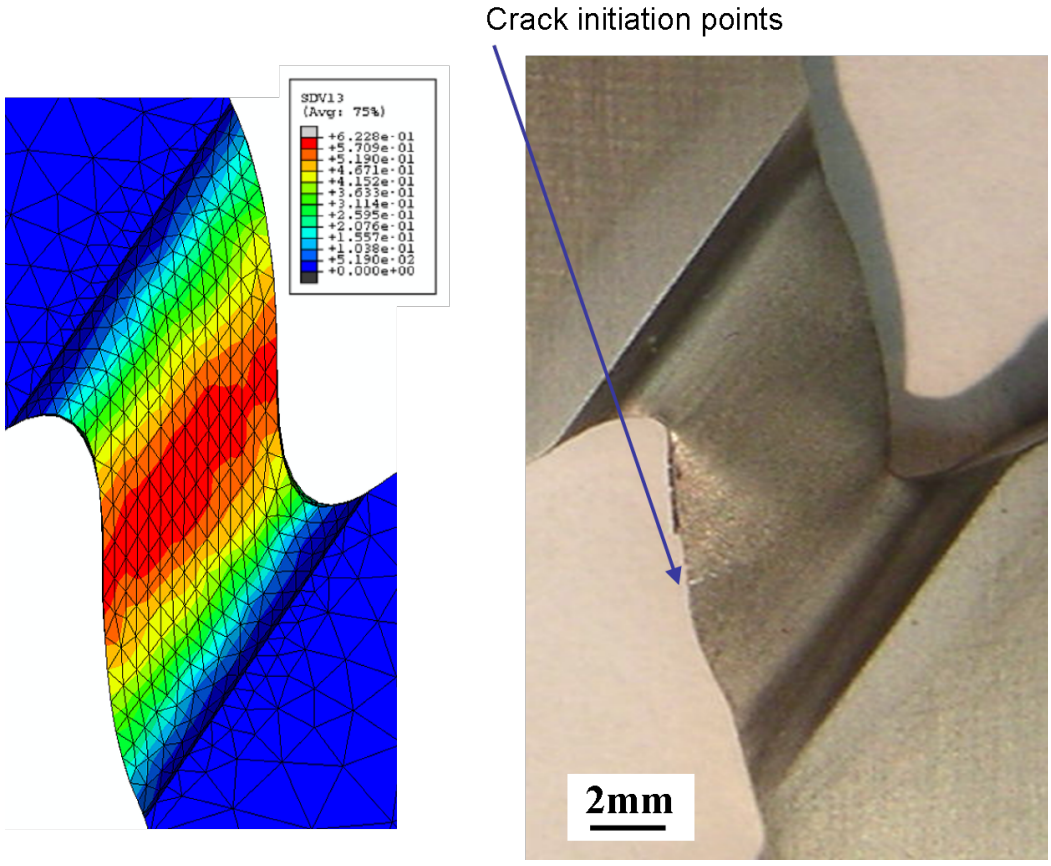

Figure 5.10: The shear+more-tension specimen at the onset of fracture (right); effective plastic strain, $\bar{\varepsilon}^p$ (left)

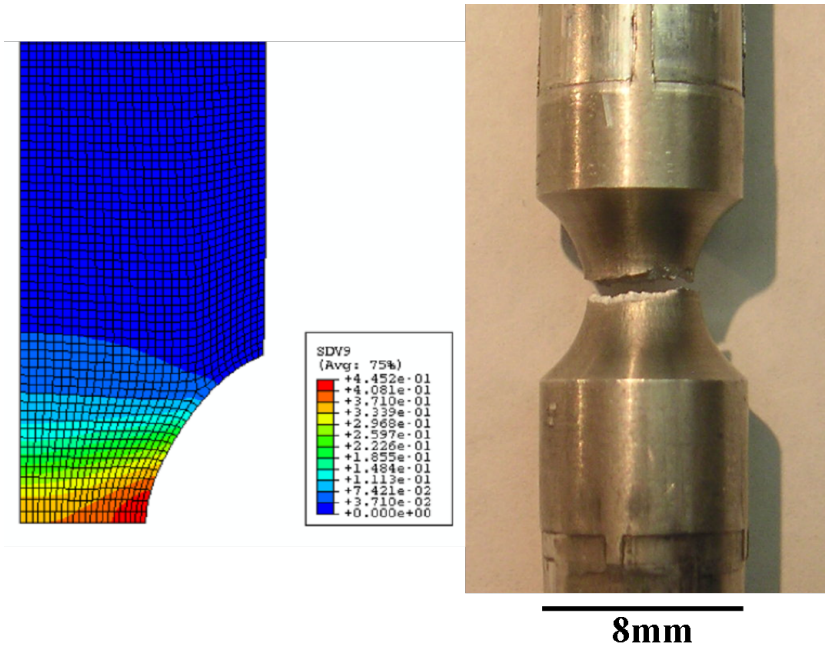

Figure 5.11: Notched cylinder with a radius of 4mm at the onset of fracture (right); effective plastic strain, $\bar{\varepsilon}^p$ (left)

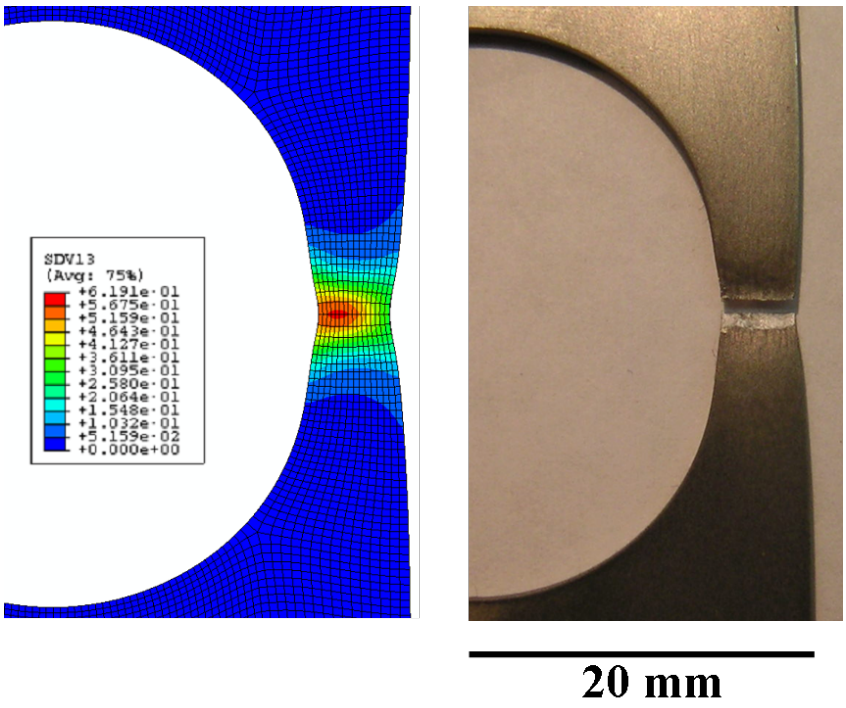

Figure 5.12: Thin plate with a hole at the onset of fracture (right); effective plastic strain, $\bar{\varepsilon}^p$ (left)

Having an estimate of the total plastic strain developed in each test, gained through combining DIC data and finite element predictions, a plot of fracture strain vs. stress triaxiality is developed. This key result is shown in Figure 5.13. The point of interest here lies in data with triaxiality values less

than 0.4. Traditional models for the evolution of ductile damage predict a monotonically increasing fracture strain with decreasing triaxiality. Here, through hard experimental evidence, it is evident that the presence of shear *accelerates* failure as triaxiality *decreases* below this value of 0.4. The trend is consistent with results for finished 2024 plate. Note that the stress state at the edge of rolled slab, where cracking develops, is in this "shear + low triaxiality" regime.

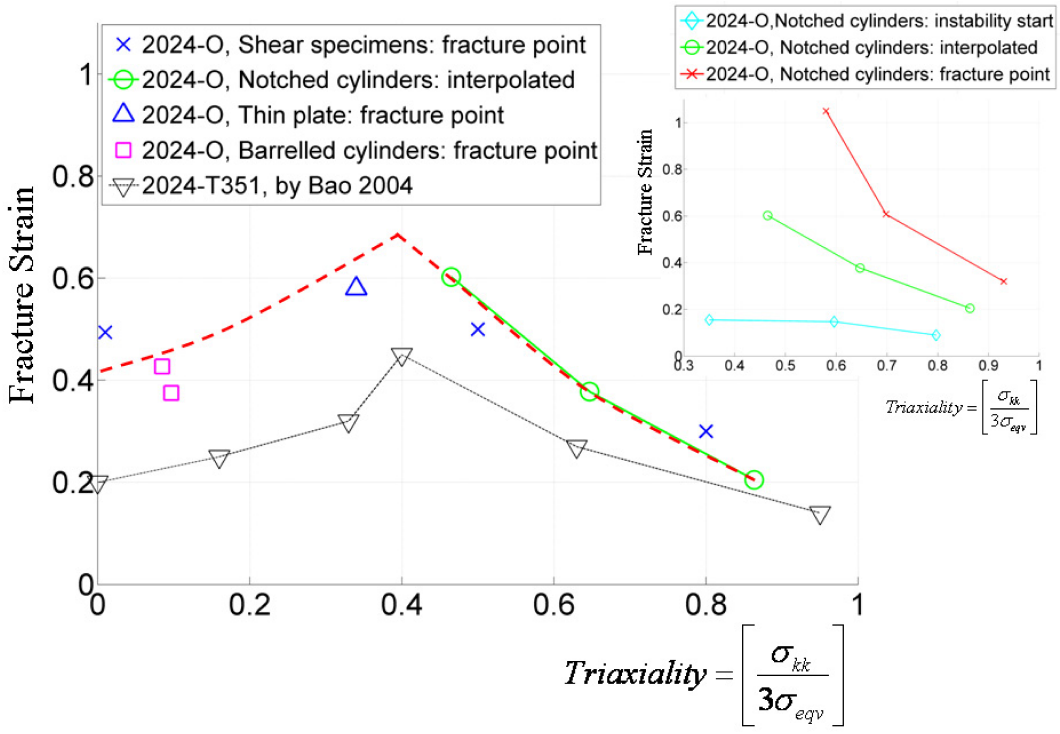

Figure 5.13: Fracture strain vs. stress triaxiality

This very complete data provides for the detailed validation of mesoscale models for damage evolution – those models being a deliverable of the study.

Task 2 Microstructure Based Constitutive Modeling and Failure Criteria Development

The development of fracture and failure criteria for aluminum at high temperature requires the combined experimental & computational studies, involving the laboratory-scale coupon tests, and the use of multi-scale computational models in Task 1.

Validation of Constitutive Model for Flow Stress Shown in Figure 5.14 are the displacement and strains measured using Digital Image Correlation (DIC) for the particular experimental case of Figure 5.5 (above). Also shown is the comparison of load vs. displacement for experiment and simulation. The simulation in this case was developed in the specimen design, and serves to confirm that the work hardening model indicated in Figure 5.2 is reliable.

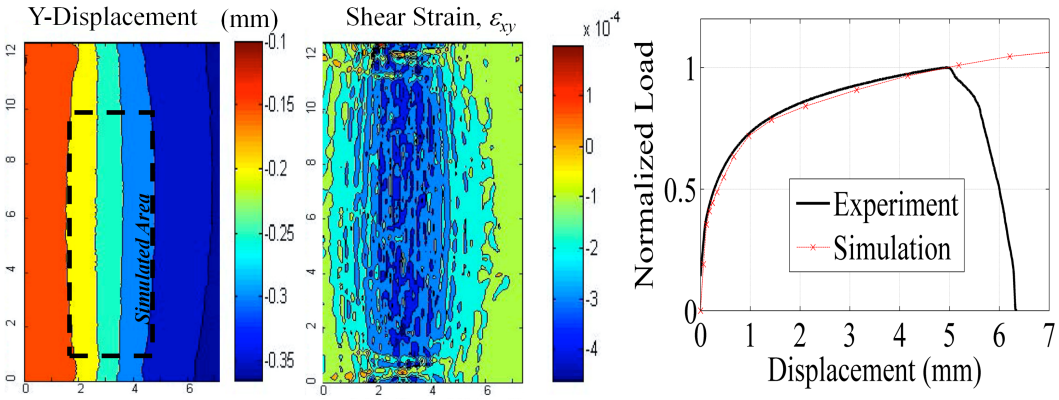

Figure 5.14: DIC results, at 0.4 mm pin displacement (left, center pictures), normalized load vs. displacement curves from the machine and the simulation (right picture).

The displacement field in the dotted box in the left-most plot provided the boundary conditions for the simulation. The displacement field at 0.4 mm of pin displacement was chosen to check the stress field and deformation patterns at an initial stage of the test, *i.e.*, to avoid any geometric inhomogeneous effects that take place at the later stages of the test. The load-displacement curve shown in Figure 5.14 indicates that the 0.4 mm pin displacement corresponds to the fully plastic stage, well past the linear elastic region. No displacement boundary conditions were specified in the out-of-plane direction in the simulation (plane stress).

Model for damage evolution through grain interaction As noted above, derivation of the mesoscale model is detailed in the thesis by Dr. S. Kweon (2009). A finite element discretization of the microstructure is posed with crystallographic orientation assigned to the individual grains represented in the mesh. Boundary displacements corresponding to the conditions of Figure 5.14, above, are introduced and the evolution of a damage parameter, Ø, is followed through the course of the simulation. Local concentration of hydrostatic stress, the driving force for damage growth, follows from grain interaction (Figure 5.15a). As a consequence, damage develops leading to local increase in a few grains (Figure 5.15b). This mesoscale model forms the basis for the implementation in the WARP3D code, to be applied to the problem of crack turning in Task 4, below.

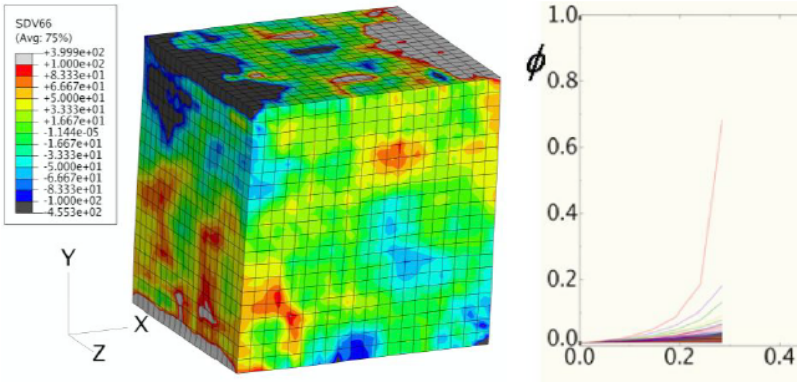

a) hydrostatic stress b) damage vs. time

Figure 5.15: a) mesoscale model for damage evolution in shear; a) local hydrostatic stress from grain-to-grain interaction, and b) growth of damage parameter vs. time (t=0.285 corresponds to a plastic strain of 0.0274.

Instabilities developed in another alloy subject to edge cracking is provided in the publication by Mudrock, R.N., Lebyodkin, M.A., Kurath, P., Beaudoin, A.J. and T. A. Lebedkina (2011), "Strain-rate fluctuations during macroscopically uniform deformation of a solution-strengthened alloy , *Scripta Materialia, v* 65, pp. 1093–1096.

5.3 Task 3 - 3D Process Modeling of the Rolling Operation

The microstructure-based computational model and failure criterion developed in Tasks 1 and 2 is used in the 3D process modeling of aluminum in hot rolling. The incorporation of these models ensures that the 3D processing includes the effect of microstructure, evolution, and the detection of crack nucleation or surface defect formation.

Model of the Hot Rolling Process using ALE3D A 3D model of AA 5182 aluminum slab, work rolls and tables has been implemented in the parallel computing code ALE3D (developed at Lawrence Livermore National Laboratory). Shown in Figure 5.16 are key components of the model. The model was developed with verification checks along the way, to establish the development of steady state conditions in a computationally manageable setting**.**

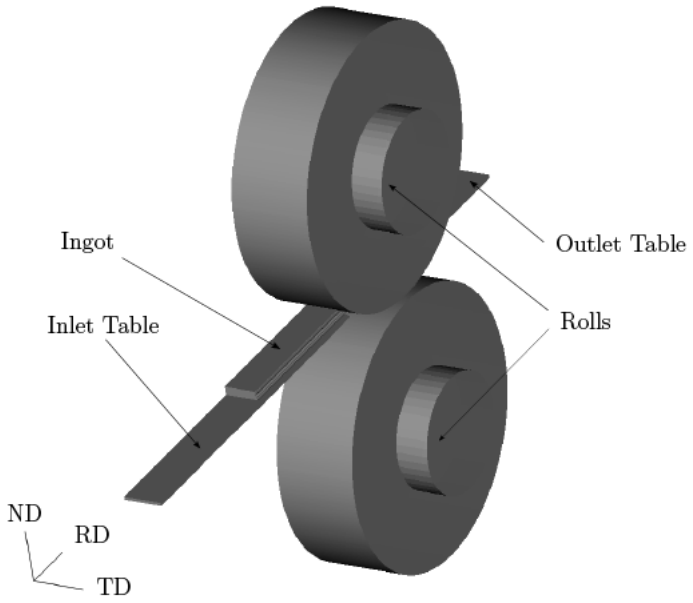

Figure 5.16: model components

Effort is centered on simulation of the passes where edge cracking is typically developed. The initial edge profile was derived from slab taken from a production rolling facility. As we begin our modeling after 25 passes, an initial condition for the damage variable was developed so as to account for previously developed damage. Based on estimates of temperature, effective strain and pressure from production data, the initial accumulation of damage is prescribed through the initial value of the damage evolution variable. The slab edge profile and initial mesh with prescription of damage are shown in Figures 5.17 and 5.18, respectively.

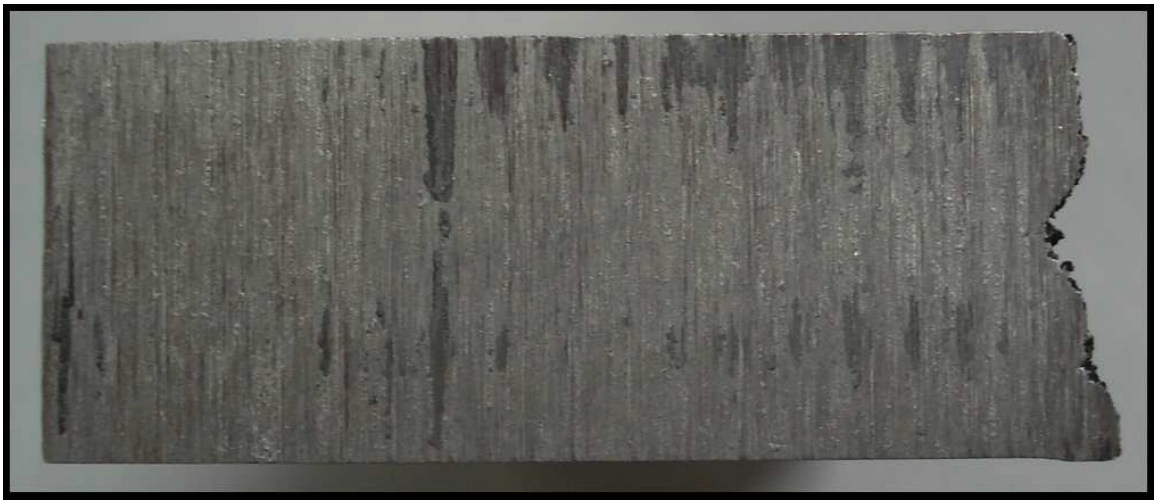

Figure 5.17: edge portion of rolled slab

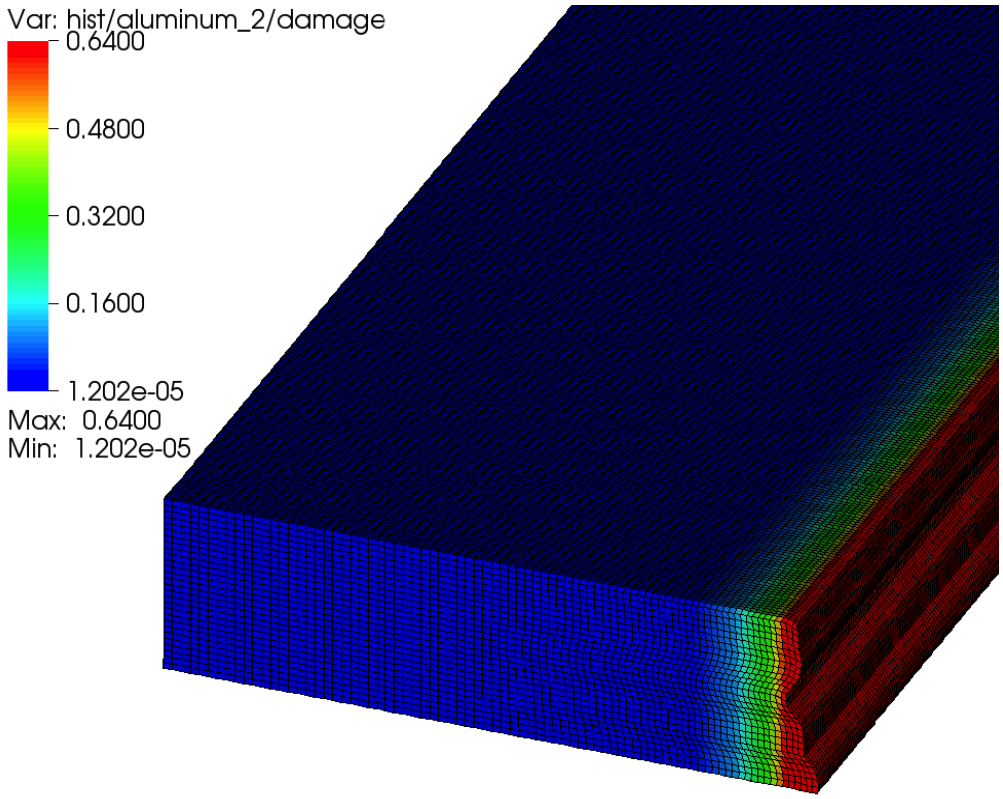

Figure 5.18. mesh for the slab with initialization of damage variable, as based on prior rolling history

Simulations reveal the development of a tensile stress component in the rolling direction (Figure 5.19), as well as the development of a negative (tensile) hydrostatic stress at the slab edge – while in the roll bite (Figure 5.20). As a consequence, cracks are initiated on the bottom surface of the ingot and propagate both inward and upward. The initiation of cracks consistently occurred on the bottom surface slightly in from the edge (Figures 5.21 & 5.22), which indicates that the geometry of the ingot in this region is prone to the development of the tensile hydrostatic pressure that drives damage evolution.

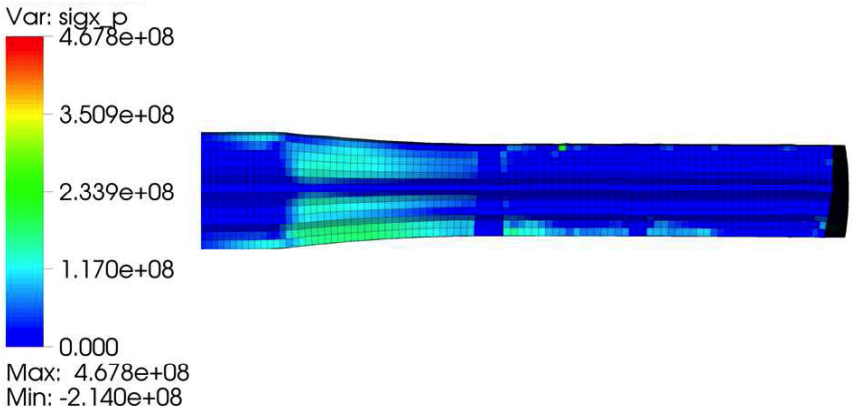

Figure 5.19: Component of tensile stress in the rolling direction

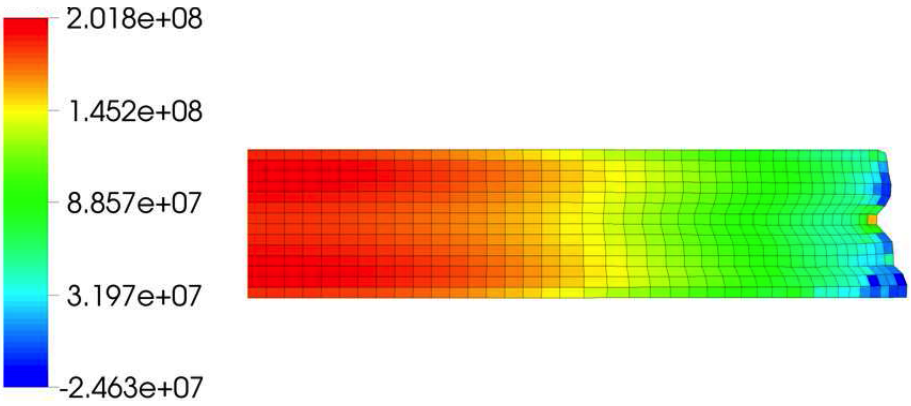

Figure 5.20: Pressure in slab cross section, as observed halfway through the roll bite, note regions of tensile hydrostatic stress at the edge (blue)

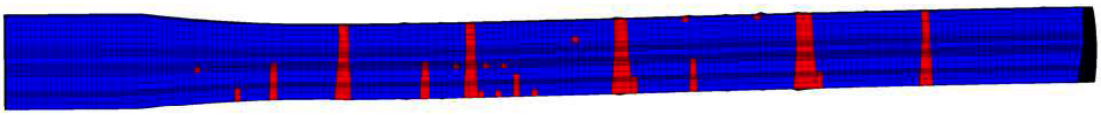

Figure 5.21: Edge cracks viewed from the ingot edge

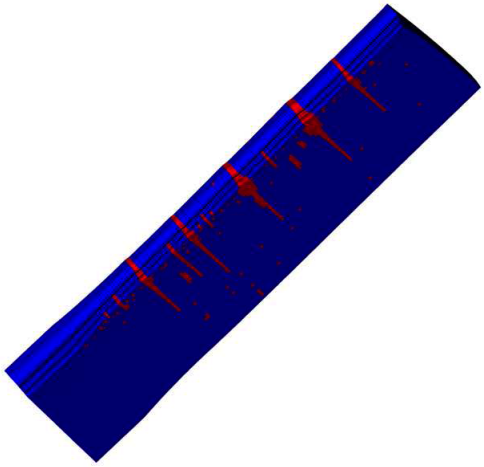

Figure 5.22: Edge cracks viewed from the bottom surface

Taken together, these results demonstrate the capability to develop a realistic geometry of the edge profile for rolled slab, develop a stress state with a tensile state of hydrostatic stress, and drive the evolution of damage in a realistic manner.

Integrated Model for Analysis of Rolling The ALE3D code, developed at LLNL, has been used to model the production rolling process (above). To provide a second, more general and pre-competitive pathway to industrial application, we have distilled the key elements of the mesoscale model into a combined material model & failure locus that may be utilized through a variety of finite element codes used by our industrial partner (and more generally used in industry). This approach combines experimental observations and results from detailed mesoscale models for damage into a computationally efficient and practical simulation procedure. As a practical end, the 'pre-competitive' character of the project deliverable is furthered: the more general and efficient approach to coding extends the practical utility to analysis beyond the hot rolling process. Specific properties of this materials property model are as follows:

- The constitutive response for AA2024-O includes logic to switch between "high temperature/low strain rate" and "low temperature/high strain rate" behavior (Kweon, Beaudoin, Kurath, & Li, 2009). The physical basis for the change in response is due the presence of solute in these alloys. This transition in behavior can be seen in Figure 5.23.

- A damage locus relating triaxiality and strain to failure are developed using a mesoscale model. In past reports, we have shown that local interactions between grains create hydrostatic stresses that drive damage processes (Kweon, Beaudoin & McDonald, 2010; Kweon, 2012). The output of the mesoscale model – that is, the strain to failure vs. triaxiality relation – is coded in the VUMAT. [Here, triaxiality is defined as the (negative) pressure divided by the effective stress.]

- A "triaxiality weighted" plastic strain (TWPS) is integrated as an internal state variable. This weighted strain measure was developed through the experimental program aligned with the mesoscale modeling effort.

- The TWPS is compared with the mesoscale-derived failure locus, and a damage variable is set upon failure.

- The allied equations for thermomechanical response is of general utility and may be introduced into many of the modeling codes used by industry. One example is the crack growth code WARP3D (Task 4, below).

This approach allows for the condensation of detailed mesoscale studies of damage evolution into a simulation procedure that is quite practical for industrial application. A further benefit is that any (appropriate) mesoscale damage model may be used to develop the failure locus.

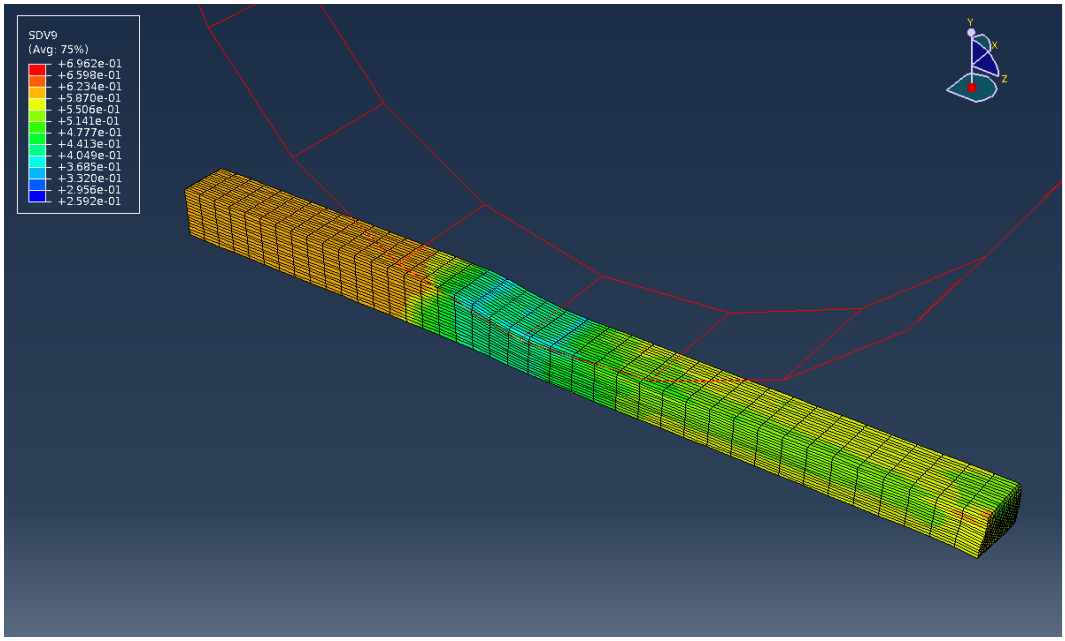

Figure 5.23: Kinetic parameter from horizontal axis of Figure 1. Note the transition from "Hi T" to "Low T" behavior in the roll bite region.

Analysis of Edge Cracking Production variables such as lay-on temperature, rolling speed, and profile of the edge of the rolled slab may be explored in the simulation of rolling. An example of an "overhanging" profile is shown in Figure 5.24. Here, there is a slight bulge that develops at the top and bottom surfaces of the slab – as a result of prior rolling. The top half of the slab is shown (by virtue of symmetry). Tensile stresses (stresses in the rolling direction, as plotted in the Figure) are evident on the slab surface in the entry and exit of the roll bite. These stresses are prominent in the bulge at the side, within the roll bite region. Such a trend offers insight into the mechanical origin of edge cracking: a side bulge, locally unsupported on bottom/top surfaces, acts as a tensile bar – with tension effectively applied along the rolling direction – as indicated several times earlier in this report.

This mechanical foundation has been the practical basis for the experimental and mesoscale modeling approach adopted in the present project. The interaction between grains at a length scale of tens of microns leads to locally high stresses, and this result is distilled into the failure locus in the VUMAT. This in turn provides consideration of grain scale interactions in a practical industrial application (showing low triaxiality at a length scale of millimeters). The predication of damage using the failure locus is shown in Figure 5.25. There is a stress triaxiality of roughly 0.4 developed in the roll bite. This is a relatively small value, if considered in light of the usual damage models. Figure 2D highlights the development of damage (leading to cracking).

In summary, mesoscale models have been developed for production aluminum alloys. These models may be exercised for the deformation states typical of rolling, providing a failure locus. The failure locus is considered in the production simulation through a material subroutine (VUMAT). Such an approach enables broad dissemination to industry and very practical computation times.

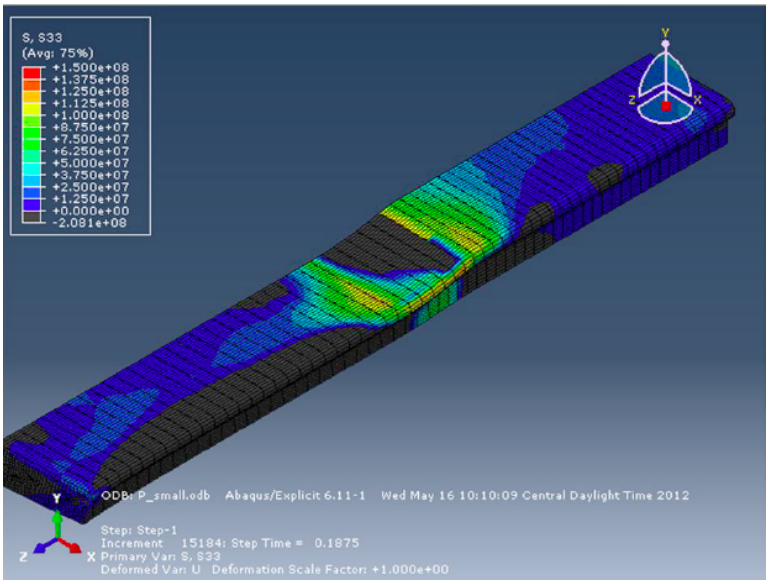

Figure 5.24: 3D simulation of plate rolling with natural overhang. Stress in the rolling direction (Z) is shown. The direction of rolling is from the upper right to lower left. The roll bite region is roughly in the center, and the slab is being compressed in Y.

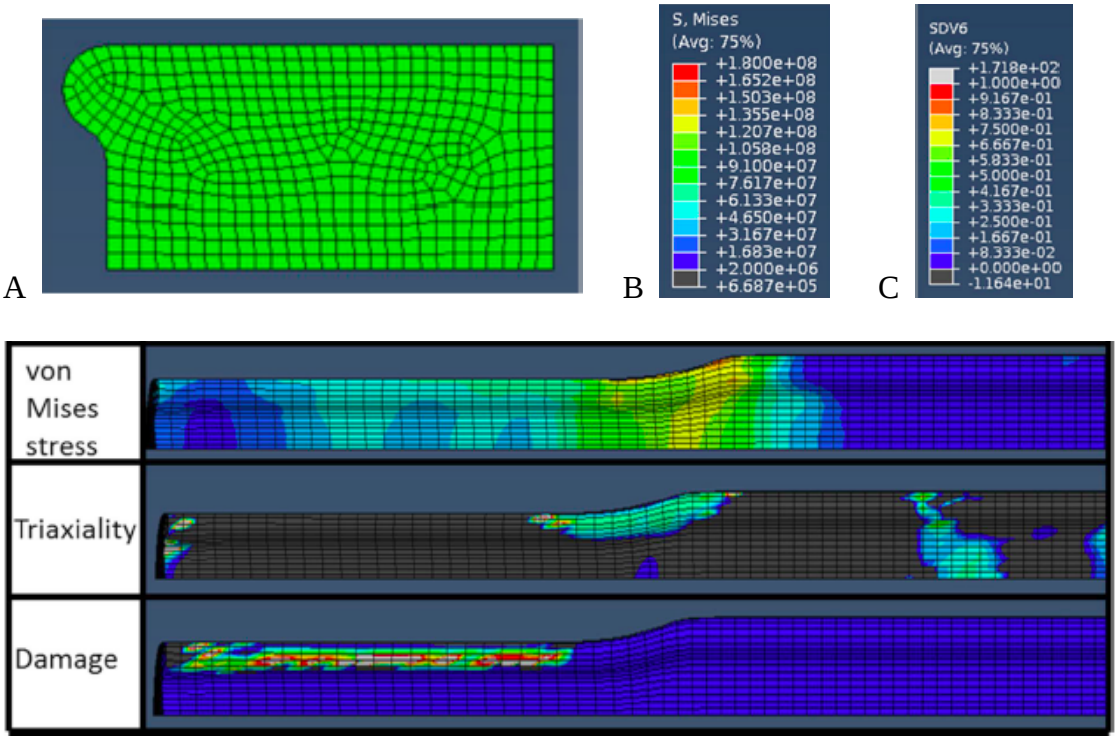

Figure 5.25: Simulation results with natural overhang, as shown in Figure 1. A) Initial mesh of cross-section with overhang; B) scale for effective (von Mises) stress; C) scale for stress triaxiality and damage (with color shading from 0/blue to 1/red; D) plots of effective stress, triaxiality and damage.

Parametric Study A parametric study has been performed using the model for the production rolling process. Parameters varied were

- Lay-on temperature
- Geometry of edge profile
- Friction coefficient
- Asymmetric rolling

Details of this study are provided in the thesis by Ms. Katherine Halm (Halm, 2012). An example of asymmetric rolling is shown in Figure 5.26. The top roll is moving faster, with respect to the bottom roll. Only the section of the mesh between the work rolls is shown. The asymmetry of the stress is evident. The resulting stress triaxiality, which drives the growth of edge cracking, is asymmetric as well.

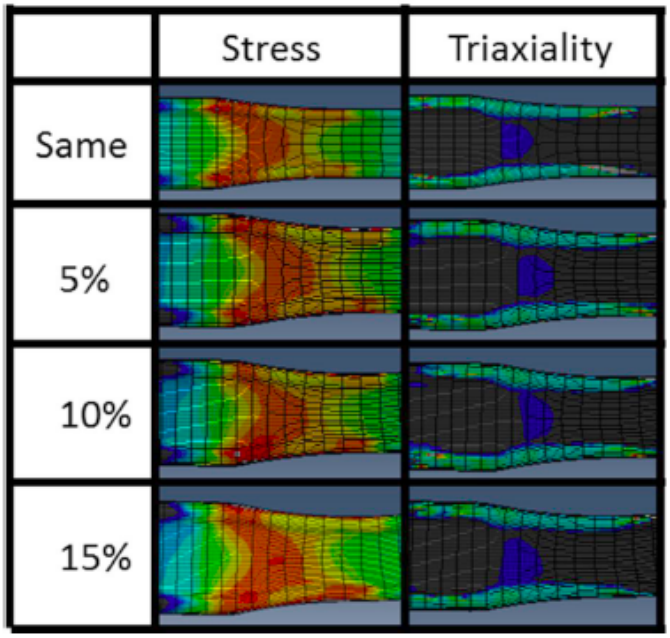

Figure 5.26: – Development of effect stress and triaxiality in the roll bite region.

Task 4 – Validation at Production Scale

In this task, the mesoscale model is implemented in the open-source code Warp3d, applied to the problem of crack turning in the hard aluminum alloy AA 7050, and validated against experimental test specimens fabricated from production alloy plate.

Mechanical Testing The stress-strain response was developed using the screw-driven mechanical load frame, with temperature chamber, at UIUC. The stress-strain response is shown in Figure 5.27a. Two key parameters are needed for the Mechanical Threshold Stress (MTS) model implemented in the WARP3D material model: the initial flow stress and the hardening rate. The initial flow stress is somewhat different than the yield stress, in that this initial stress value is tied to the onset of a linear decrease in the work hardening rate – and not the usual 0.2% offset criterion.

The hardening rate, θ, is defined as

$$\theta = \frac{\partial \sigma}{\partial \varepsilon}$$

where σ is the true stress and ε is the true strain. This hardening rate is the instantaneous slope of the stress-strain curve. The MTS model is based on a linear decrease in the hardening rate with stress. The objective of the present effort is to establish the initial stress and linear hardening rate to be entered into the material model coded into WARP3D.

The hardening rate is plotted in Figure 5.27b. A linear trend is evident. There are some superposed oscillations, and these may possibly follow from the action of solute on dislocations. For a material with no precipitation hardening (a pure fcc metal), the initial hardening rate would be equal to the elastic modulus divided by 50; for aluminum this is 72,000 [MPa]/50, or 1440 [MPa]. The fitted portion of the curve varies linearly with stress, and the fit is quite good with an R^2=0.985. This linear region is developed at a yield stress of ~460 MPa and a hardening rate of 2000 [MPa] – just a bit greater than would be expected for pure aluminum and quite reasonable. ***These values for the initial flow stress, the initial hardening rate, and the slope following from the linear fit are the critical parameters required for the material model in WARP3D. The validation of the material model, as implemented in WARP3D, is given in Section 7.*** Also shown are the elasto-plastic transition region (σ < 460 [MPa]) and the onset of localization (σ > 505 [MPa]). The Considere criterion for localization in a tensile test,

$$\sigma = \frac{\partial \sigma}{\partial \varepsilon}$$

is plotted as a dashed line. The localization observed in the experiment occurs just prior to the (theoretical) Considere criterion.

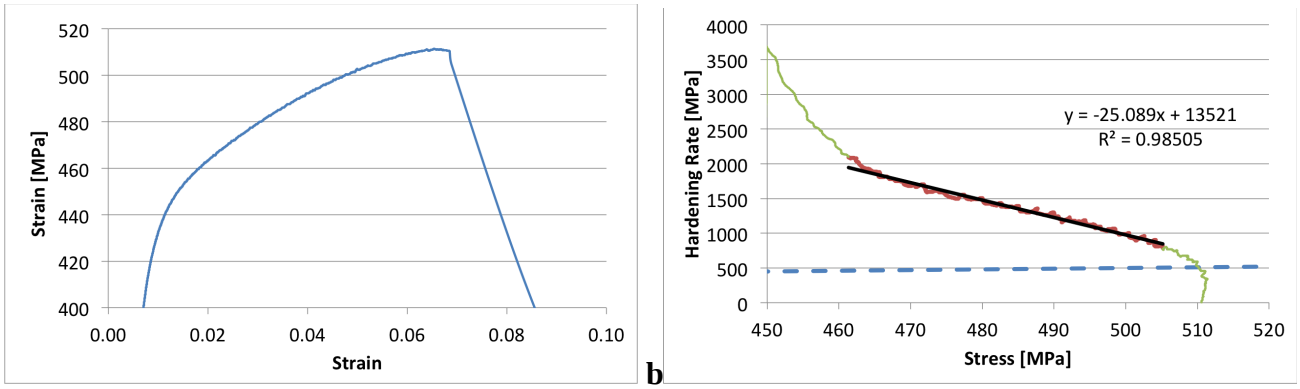

Figure 5.27 – Mechanical testing data for AA 7050: **a**) stress strain curve; **b**) hardening rate derived from stress-strain curve. The fitted portion of the curve varies linearly with stress. Also shown are the elasto-plastic transition region (σ < 460 [MPa]) and the onset of localization (σ > 505 [MPa]). The Considere criterion is plotted as a dashed line.

Following from the experiment procedure described above, there are two components supplied to the material model: a 'yield' strength and a saturation stress (which, in turn, provides for the work hardening). These parameters are derived from mechanical tests performed at both ATC and UIUC.

- The **yield stress**, normalized by the shear modulus, is plotted in Figure 5.28a. The yield stress is determined from the point at which the hardening rate data meets the linear fit shown in Figure 5.28b (a value of roughly 460 MPa in that particular plot). Data is plotted for both the peak- and over-aged tempers, and also for different thickness locations through the plate. The

key feature of fitted curves in these plots is the horizontal character of the lines. This indicates an essentially athermal response, that is, yield is relatively insensitive to changes in strain rate and temperature. This athermal strength likely represents the resistance provided by the precipitates developed through tempering.

- The second portion of the material model relates to the **work hardening**. Here, a saturation strength is required: the difference between the yield stress and the the stress level at which the stress-strain curve becomes 'flat' (the rate of strain hardening is zero). This is developed by the extrapolation of the fitted line in Figure 5.27b to the horizontal (x) axis. *Our data analysis showed that data for all material conditions collapsed onto a single curve* (Figure 5.28b, right).

Taken together, these two observations indicate that the selection of AA 7050 as a model material for this project was quite fortuitous. For a particular heat treatment and thickness location, there is a corresponding yield strength (just a single value). Then, work hardening appears to be the same for all processing conditions. This relative simplicity aids considerably in making the connection between processing conditions and fracture, the overarching goal of this project. The material parameters for the four process conditions are complete, as are the finite element meshes. Driving forces have been studied for a variety of conditions (e.g. high/low anisotropy).

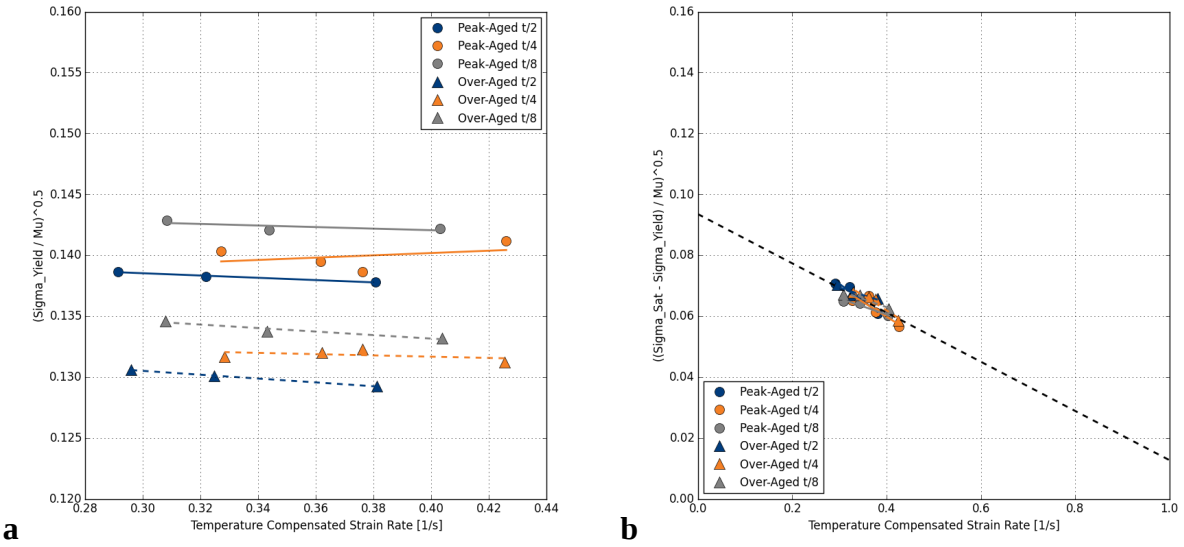

Figure 5.28 – a) Yield stress, normalized by shear modulus, for plate in peak and over-aged conditions at different thickness; the near-horizontal fits to data indicate a rate-insensitive behavior. b) The rate-dependent response of the saturation stress for both aging conditions at three thickness locations; all data collapses to a single curve.

Synchrotron Studies To provide a useful, *or rather predictive*, model for crack deviation there must first be sound physical insight into the mechanisms driving the fracture process. Further, to make the connection between application and process, these mechanisms must be understood at the scale of the microstructure. In this project, ***discovery*** of the specific conditions that promote asymmetric deformation at the mesoscale were made through studies conducted at Sector 1 of the Advanced Photon Source (APS) of Argonne National Laboratory.

Synchrotron Study #1: Development of local tensile hydrostatic stress A first synchrotron study provides an indication as to just how significant the local development of tensile hydrostatic stress can be at the mesoscale. [It is this local variation of hydrostatic stress that forms the basis for damage evolution adopted in this project.] This work is detailed in the peer-reviewed publication, Beaudoin, A. J., Obstalecki, M., Tayon, W., Hernquist, M., Mudrock, R., Kenesei, P., Lienert, U. (2013). In Situ Assessment of Lattice Strain in an Al-Li Alloy, *Acta Materialia* 61, 3456-3464.

Shown in Figure 5.29 is the stress history for three grains tracked in the experiment. The deviatoric stress, **s**, is shown, where

$$s = \sigma - \sigma_m I$$

and the mean stress is $\sigma_m = \sigma_{ii}/3$. The measured nominal tensile stress, σ_t , based on the undeformed cross section is plotted as a dashed line in the plots. The sum $\sigma_{zz} = s_{zz} + \sigma_m$ is plotted as a solid line without symbols and follows the same general trend as the tensile stress (with expected grain-to-grain variation).

Of key interest, from the viewpoint of damage evolution, is the marked difference in stress triaxiality for these three grains. Here, triaxiality is taken as $\frac{\sigma_m}{\sigma_{eff}}$ with the effective stress $\sigma_{eff} = \sqrt{\frac{3}{2} s : s}$. A plot of effective stress plotted against the tensile stress is shown in Figure 5.30. Over the initial course of loading, there is striking agreement between the data for the 'hard' grain C and a reference curve (indicative of a purely elastic loading). As yielding occurs, at a stress of roughly 550 MPa, the effective stress for this grain then increases relative to the measured tensile stress, while the other two grains show effective stress that falls below. This offers some indication that the grain C is accommodating the applied load primarily through an elastic deformation, in contrast to elasto-plastically deforming grains A and B. There is a concomitant unloading of the hydrostatic stress for grain C during the bulk elastoplastic transition, leading to the relatively lower triaxiality for that grain.

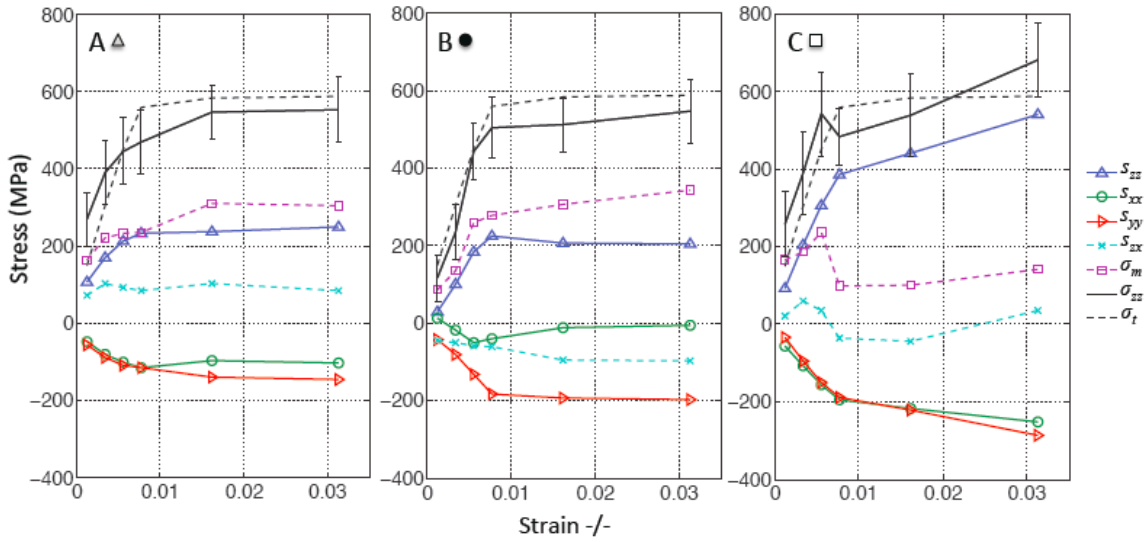

Figure 5.29 – Stress history for three grains during tensile loading.

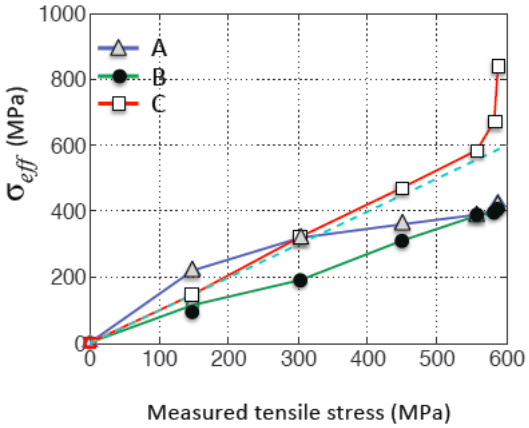

Figure 5.30 - Effective stress plotted against the measured tensile stress.

It is this simultaneous presence of grain pairs where one grain is oriented favorably for slip (plasticity) and another is deforming in essentially an elastic manner that forms the basis for the model of crack turning to be described.

Synchrotron Study #2: Experiment with Stress Concentration An experiment was performed at the Advanced Photon Source of Argonne National Laboratory from July 23 through July 27, 2014. The sample material was AA 7050 provided by ATC. The experiment utilized a novel configuration of detectors at sector 1-ID:

- a 'mid-field' detector is used to map the positions of grains in the sample (figure below, the square detector with yellow tape on front);
- a 'far-field' array of four detectors in a diamond-shaped arrangement provides the resolution for determining stress in individual grains.

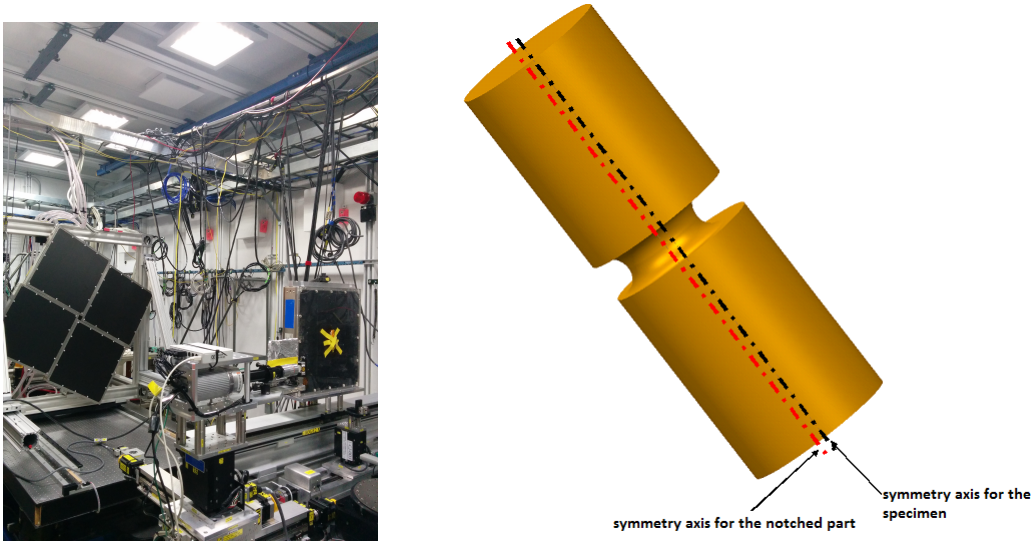

Figure 5.31: detector arrangement (left); sample with off-set loading axis (right).

The sample was designed to provide an approximation of the stress state that exists ahead of the crack tip, yet be manageable in the synchrotron environment. The sample has a notch, so as to develop the tensile hydrostatic stress that promotes damage (Figure 5.31, right). The loading axis is off-set from the specimen centerline, to provide a state of tension superposed with bending – leading to a gradient of

stress.

The location of five grains in the sample cross-section (at the mid-length of the notch) is shown at left. Results of grains 0 and 4 will be highlighted.

The component of stress in the loading (tensile) direction is shown in Figure 5.33. First, note that there is a curve with several points; this is the loading curve, where the stress state was tracked *in situ* over several small loading increments.

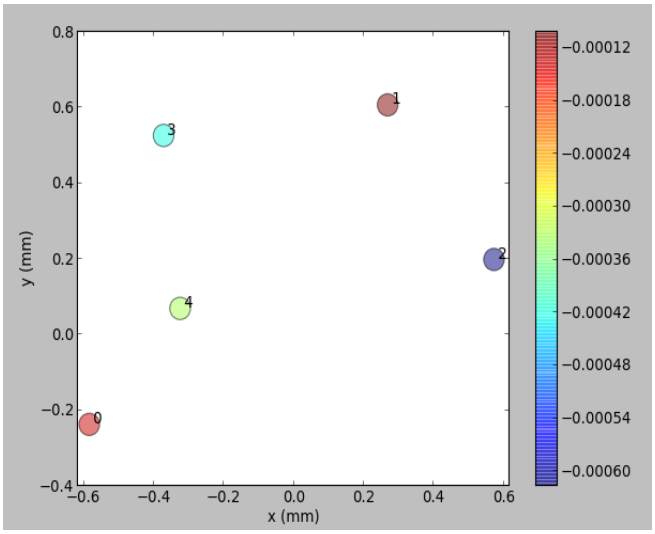

Figure 5.32: Grain locations

These incremental loading curves are followed by straight lines that show an unloading, reloading and unloading. That these curves show a return to a zero stress state for each of the two grains upon unloading is critical: this lends much confidence to the calibration procedure used to evaluate the stress in individual grains.

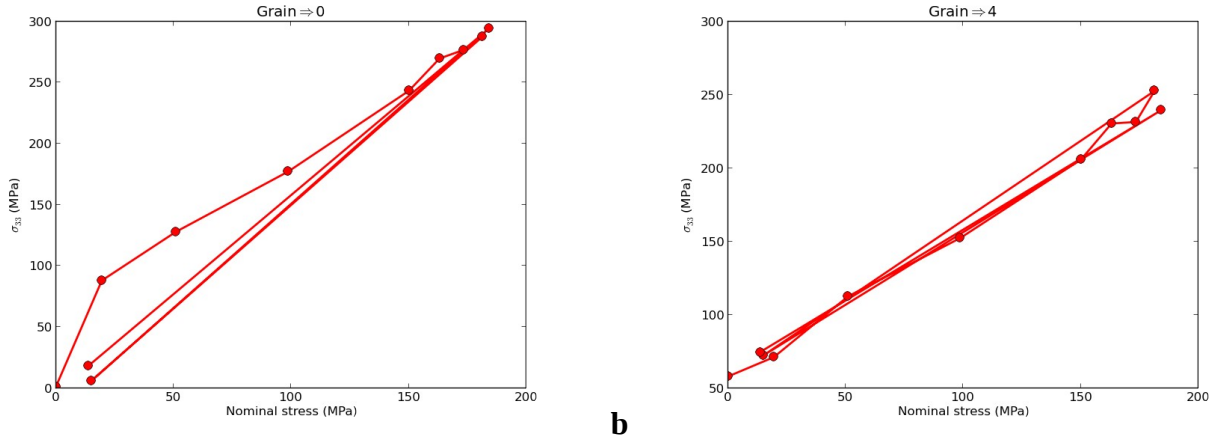

a **b**

Figure 5.33: tensile stress component along the loading axis for grains 0 (a) and 4 (b). The vertical axis gives stress measured through x-ray diffraction; the horizontal axis is a nominal stress measured with a load cell.

Grain 0 shows the larger tensile stress component. This is a grain near the edge of the specimen, located in the presence of a superposed (tensile) bending stress. A measure that is critical to the development of damage in the alloy plate is the stress triaxiality – the ratio of effective stress to tensile hydrostatic stress. [In theories of damage, the measure of porosity evolves as a function of the stress triaxiality.] The history of stress triaxiality for the two grains is show in Figure 4, below. As a point of reference, the value expected for a routine tensile test is 1/3. The stress triaxiality for both grains is on the order of 1, which is quite high and shows the effectiveness of the notch in the specimen design.

The significance to the present research is the 'shedding' of the stress triaxiality from one (hard) grain to another (soft) grain in the presence of a stress concentration. While grain 0 shows the

higher tensile stress (Figure 5.34), a decrease in stress triaxiality is shown as the sample yields plastically. A reverse trend is evident for grain 4: the grain 'picks up' triaxiality as loading precedes, rendering a state more prone to damage.

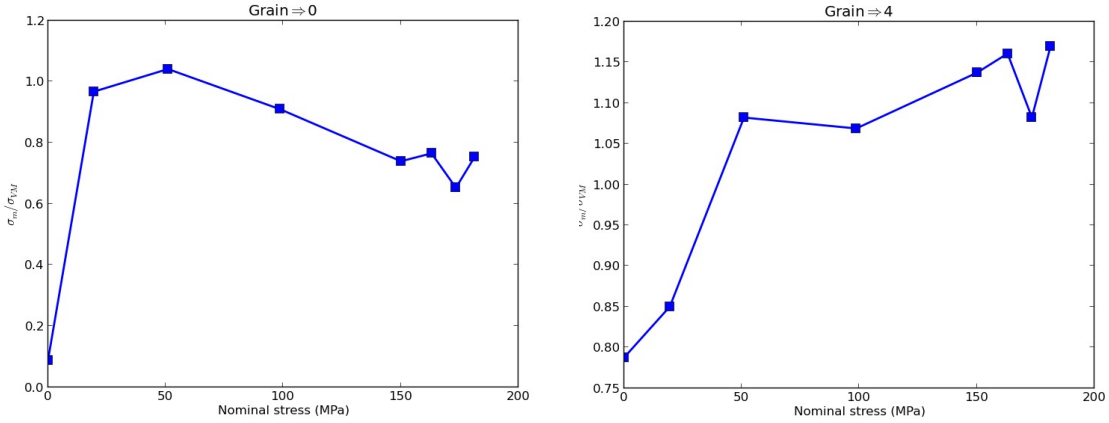

Figure 5.34: stress triaxiality for grains 0 (left) and 4 (right).

Synchrotron Study #3: Identification of Incompatibility through Synchrotron Study In October 2014, another experiment using AA 7050 was conducted at the Advanced Photon Source (APS) of Argonne National Laboratory. In this experiment, a sample with a stress concentration was loaded at Sector 1 of APS. The sample in the load frame is shown in Figure 5.35. In contrast to the study just described, the sample was symmetrically loaded and stresses were mapped at the scale of individual subgrains. The presence of the stress concentration allows for development of stress triaxiality (ratio of the hydrostatic component of stress to the effective stress associated with plastic yield). The evolution of damage, through the growth of voids, is driven by stress triaxiality. Again, it is the stress triaxiality in the region of the grain boundary that is of special concern in this project.

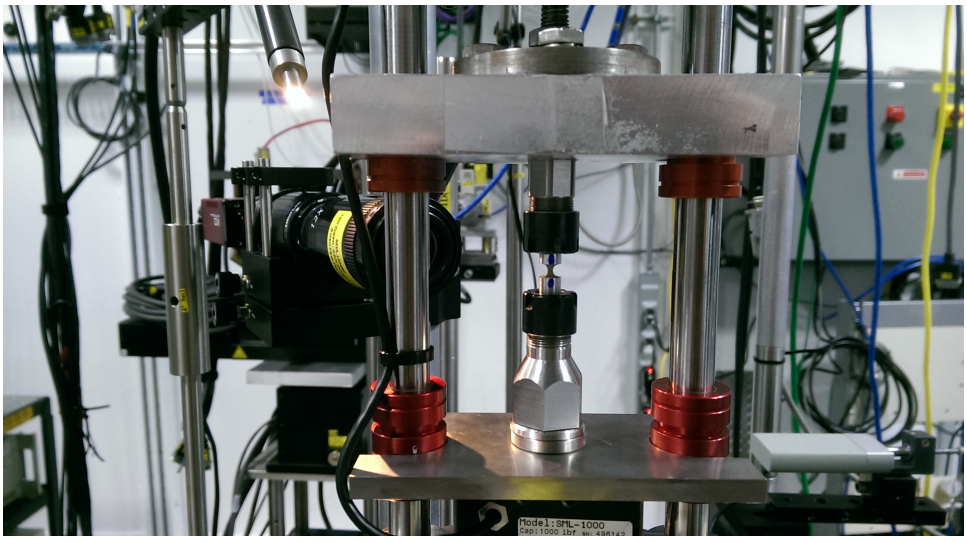

Figure 5.35 – Sample with stress concentration in loading fixture.

Two particular pieces of equipment, unique to Sector 1 of APS make this experiment unique in assessing the stress development through grain interaction: the “hydra” detector array (Figure 5.31a) and the high-resolution monochromator. The high-resolution monochromator renders a smaller energy bandwidth, which in turn enables one to discern individual subgrains of the relatively large grains in AA 7050 rolled plate. The capability to map subgrains gives particular grain boundary pairs to model damage growth.

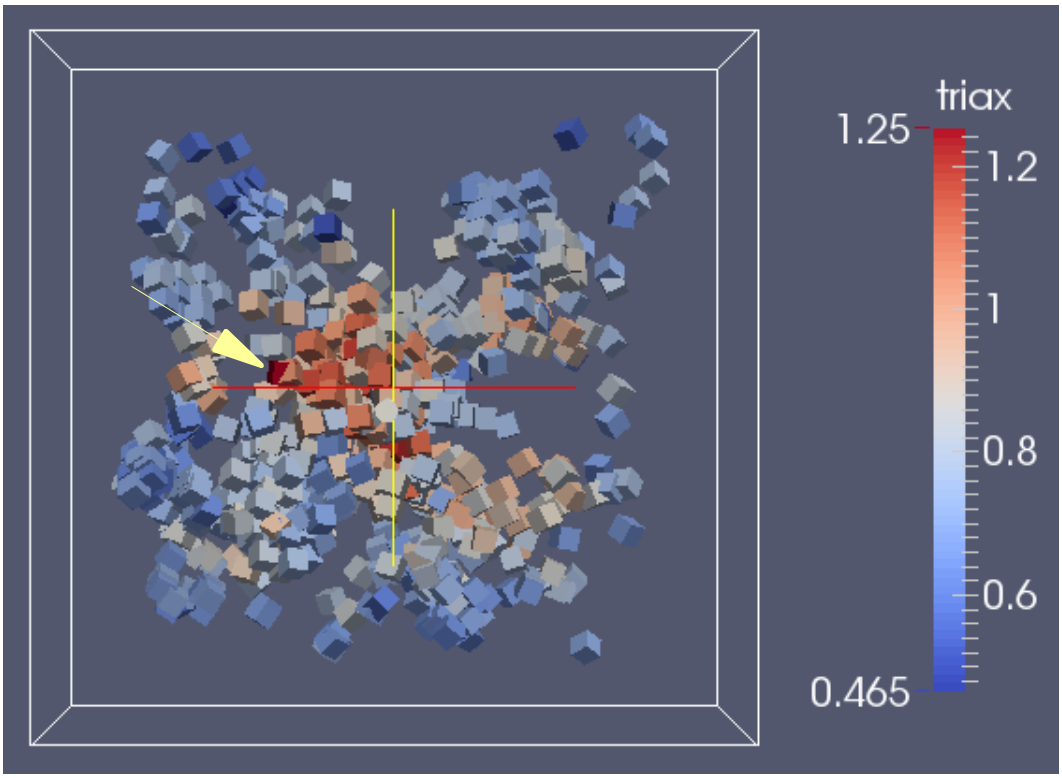

Figure 5.36 – Stress triaxiality measured through in situ study of a sample with stress concentration. Measurement made at Sector 1 of the Advanced Photon Source.

A map of the stress triaxiality is shown in Figure 5.36. The loading direction is out of the page, and the specimen cross-section is indicated by white lines. There is an elevated stress triaxiality (which drives grain boundary damage) in the center, as would be expected from theory. The advance in technique over the course of the present research is clear: in contrast to identifying a small set of grains (five), not only are many grains identified but resolution extends to subgrains. From this data, grain pairs are available to specify the crystallographic orientations ahead of the crack tip in WARP3D simulations. **The particular subgrain pair used in the simulations to be described are indicated by the (yellow) arrow. This pair of subgrains show precisely the disparity in stress triaxility that is postulated as the driver for crack turning.**

Simulations of Crack Turning

The ultimate product of this project is the development of a model for crack turning. The model has sound physical basis, with detailed documentation providing for use of the software.

One objective is to provide a ready path for use of the software by industry. In the original conception

of the project, the code ALE3D – developed by researchers at Lawrence Livermore National Laboratory – was to be used. It was found that wider distribution of the model for rolling was possible by use of the commercial finite element code ABAQUS. The material model developed through tasks 1 & 2 was implemented in ABAQUS to produce the model of cracking during rolling operations, as described in Task 3, above. Finally, the transition from ABAQUS to WARP3D enables use of open-source software within the over-arching framework of a code designed for the analysis of fracture. This choice also leverages the software and documentation developed by Prof. Dodds and collaborators over many years. This final move to WARP3D greatly facilitated the transfer to the industrial partner of this project (Alcoa).

The mesh used for the study of crack deviation in production material is described in the following publication: Messner, M.C., Beaudoin A.J. & R.H. Dodds, Jr. (2014) Mesoscopic modeling of crack arrestor delamination in Al-Li: Primary crack shielding and T-stress effect", *International Journal of Fracture*, v. 188, pp. 229-249. The finite element mesh is shown below, in Figure 5.37. The boundary layer model for the crack is given in Figure 5.37a. Boundary conditions include the capability to provide the T-stress, T_{SS}, which enables a match to actual experimental sample geometries. The mesh is highly refined just ahead of the crack, Figure 5.37b. This refinement is shown on cross section at the crack plane in Figure 5.37c, showing through-thickness refinement near crack front.

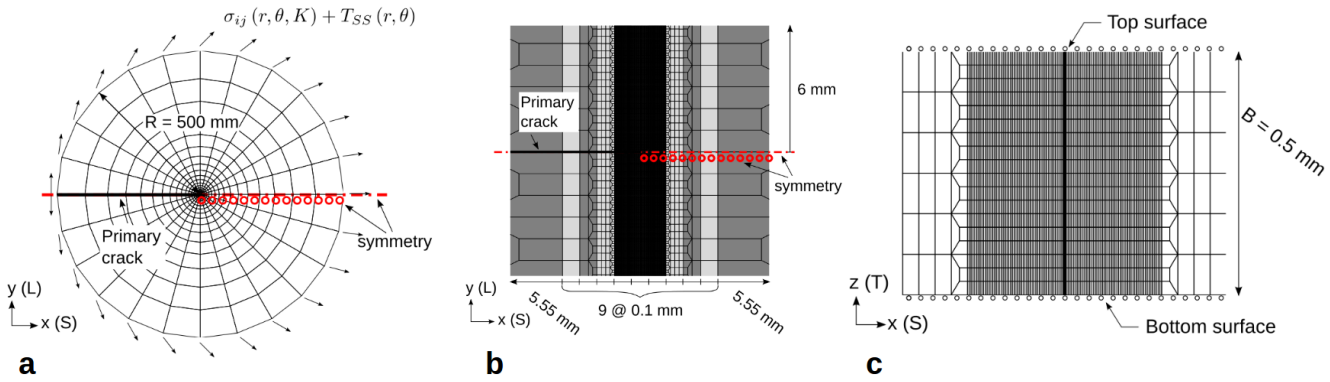

Figure 5.37 – Mesh used in finite element study of crack deviation.

In the region ahead of the crack tip, a grain orientation pair is specified. These grains alternate ahead of the crack. The crystallographic orientations for the pair of grains identified in Figure 5.36 are prescribed as grains 1 & 2 in Figure 5.38a. In Figure 5.38 a measure of the stress triaxiality is plotted, that is the ratio of the mean stress to the effective stress. This is the driving force for crack growth. The elongated grains extend vertically in this figure. A crack deviates by turning up or down along a grain boundary in the vertical.

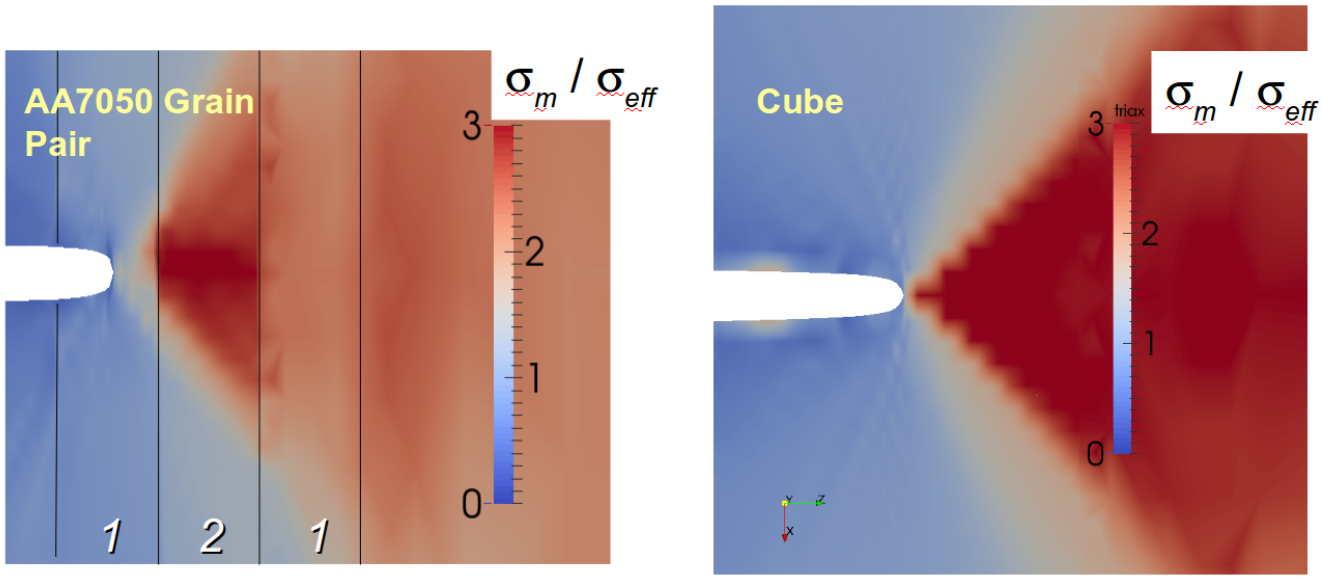

Figure 5.38 – Development of stress triaxiality ahead of the crack tip for a) grain orientations identified from synchrotron study #3, and b) a homogeneous model with a single symmetric (cube) orientation.

As a point of comparison, a single orientation is prescibed in Figure 5.38b, rendering a homogeneous material state ahead of the crack tip. It is clear that the anisotropy inherent in the grain pair suppresses stress triaxiality in the grain (1) directly ahead of the crack in Figure 5.38a, while maintaining triaxiality in grain (2). This is in contrast to the symmetric orientation of Figure 5.38b.

The mechanism for crack deviation found in this work follows from the observation of asymmetry in stress triaxiality observed in synchrotron study and the behavior of the associated grain pairs in the model for crack driving forces: anisotropy of the response pushes the region of high stress triaxiality away from the primary crack tip, where damage can develop along the grain boundary leading to crack turning.

The Rice-Tracey parameter is used as a measure of damage. It is useful to look at the individual measures that enter into the Rice-Tracey parameter,

$$\ln\left(\overline{R}/R_0\right) = 0.283 \int_0^{\varepsilon_{eff}} \exp\left(\frac{1.5\,\sigma_m}{\sigma_{eff}}\right) d\,\varepsilon_{eff}$$

where $\overline{R}/R_0$ is the void growth ratio, σ_m is the mean stress, σ_{eff} is the effective stress and ε_{eff} is the effective plastic strain. The mean stress and effective plastic strain are shown in Figure 5.39. The increase of the mean stress in grain 2 – just to the right of the crack tip, and the plastic strain developed on the boundary contribute to evolution of the void growth ratio. Note the asymmetry in the development of ε_{eff} ; this is a consequence of the anisotropy inherent in the plastic slip.

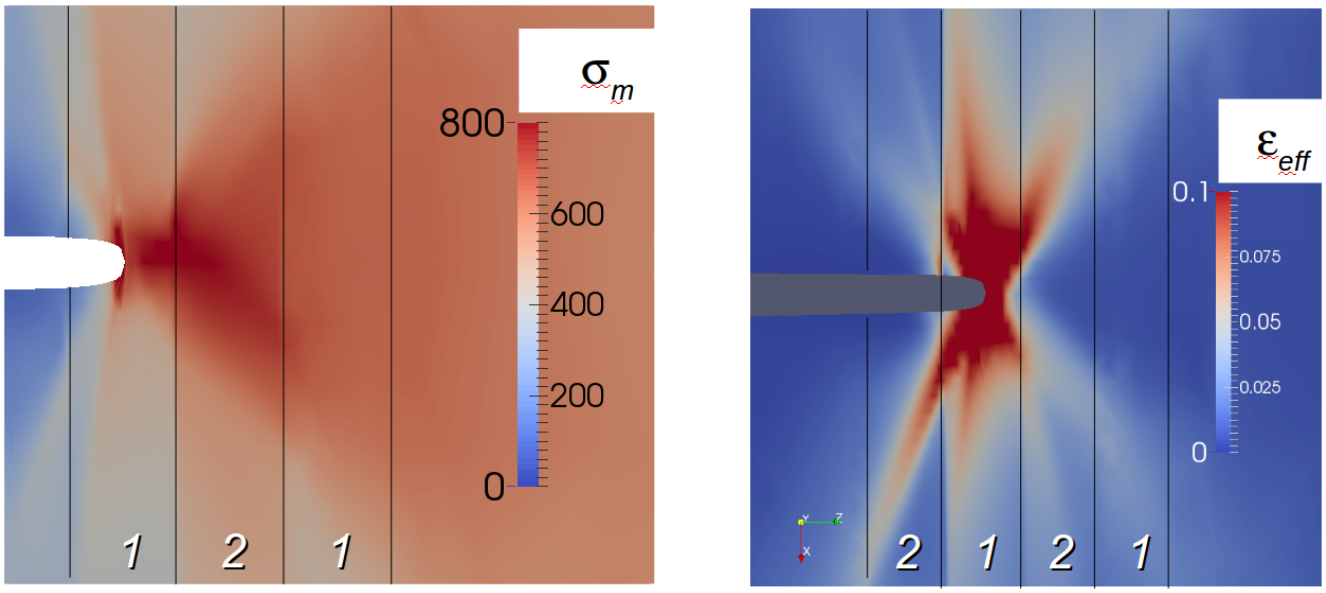

Figure 5.39 – a) mean stress and b) effective plastic strain for grain pair identified through *in situ* study at APS Sector 1.

Under this project, python scripts were developed to process WARP3D output files and generate the void growth ratio. The result is shown in Figure 5.40.

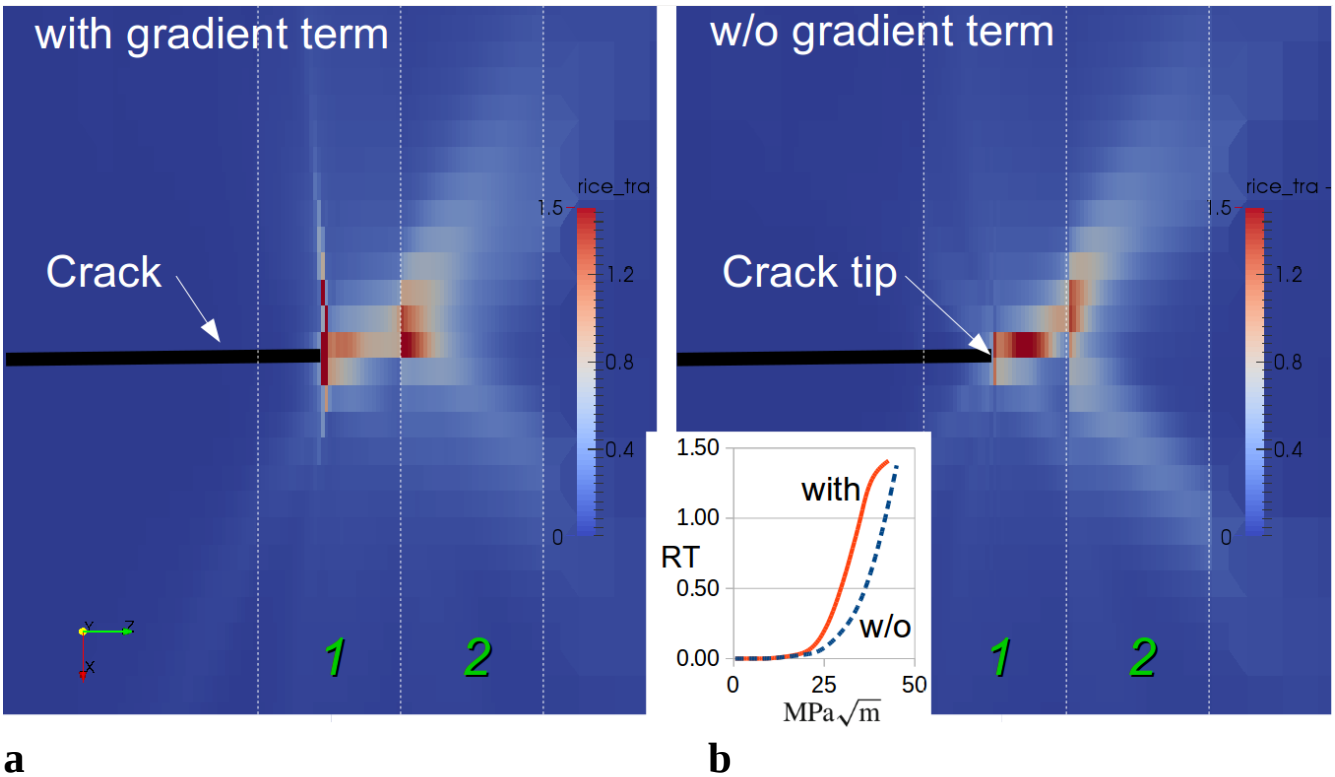

Figure 5.40 – Development of the void growth ratio (RT) a) with and b) without the gradient hardening term.

Looking at Figure 5.40b, the combined result of the elevated stress triaxiality in grain 2 (Figure 5.38a)

and the plastic strain evolution Figure 5.39b leads to damage along the boundary between grains 1 & 2, just above the horizontal containing the crack tip.

Included in the model is the a term that renders work-hardening in response to gradients in the elastic distortion. The allows for the treatment of gradients in slip that develop as a consequence of heat treatment – features of the microstructure that are too small to treat practically through refining discretization. Quite interesting, turning on this gradient further suppresses the plasticity ahead of the crack tip (Figure 5.40a).

Task 5 – Commercialization Plan

There are eight publications and four student theses that provide detailed description of both the experiments that underly the modeling effort, and the model proper. The key to commercialization of the research was to establish a pathway of to delivery (of a quite sophisticated model founded upon state-of-the-art experiments) through an open-source framework, WARP3D. In the course of the present project, both national laboratory and commercial software platforms were considered and utilized. However, *it was introduction of the parameters derived from the experimental data, detailed above, into an open-source infrastructure that was key to effective & unrestricted transfer of the technology developed in the project*.

Code Delivery to Industrial Partner WARP3D was installed at ATC by downloading from the WARP3D website and installing on the internal compute servers at the the ATC. There were regular communications between Profs. Armand Beaudoin & Robert Dodds (UIUC) and Drs. Mark James and Po-Yu Chang to install latest releases with the crystal plasticity model. Simulations performed at UIUC were reproduced at ATC. Support scripts to post-process dataset were developed in Python and provided as part of the present work. ATC researchers have further developed specialized post-processing codes in Python to extract/present/manage detailed results from the computations. Beyond the specific goals and objectives of the present work, Drs. James and Chang are employing WARP3D and the unique crystal plasticity modeling capabilities to improve understanding of fundamental deformation mechanisms in Al alloy systems at the physical length-scale of individual grains.

Dr. James has communicated with Prof. Dodds a number of times about ongoing efforts to further the parallel scaling of WARP3D on large computing clusters to reduce times-to-completion for very large models (multi-millions of elements) in the course of parametric studies. A new 2 year, Intel Parallel Computing Center has been funded at the Ohio Supercomputer Center focused on increasing the parallel efficiency of WARP3D for large-scale industrial applications of the type performed at the ATC. The ATC interactions contributed positively to the selection by Intel to form this new center. This will only aid in distribution of the model advanced by this project.

6. Products Developed Under the Award

Publications

Beaudoin, A. J., Obstalecki, M., Tayon, W., Hernquist, M., Mudrock, R., Kenesei, P., Lienert, U. (2013). In Situ Assessment of Lattice Strain in an Al-Li Alloy, *Acta Materialia* 61, 3456-3464.

Beaudoin, A. J., Obstalecki, M., Storer, R., Tayon, W., MacH, J., Kenesei, P., & Lienert, U. (2012). Validation of a crystal plasticity model using high energy diffraction microscopy. *Modelling and Simulation in Materials Science and Engineering*, *20*(2). doi: 10.1088/0965-0393/20/2/024006

Garbaciak, T. S. (2015). Grain boundary shear in AA7050: An experimental investigation using digital image correlation and finite element techniques. Thesis. University of Illinois at Urbana-Champaign.

Halm, K. (2012). On the Modeling of Rolling: A Special Look at Edge Cracking. Thesis. University of Illinois at Urbana-Champaign.

Kweon, S. (2009) Edge Cracking in Rolling of an Aluminum Alloy AA2024-O. Ph.D. Dissertation. University of Illinois at Urbana-Champaign.

Kweon, S., Beaudoin, A. J., Kurath, P., & Li, M. (2009). Development of localized deformation in AA 2024-0. *Journal of Engineering Materials and Technology, Transactions of the ASME, 131*(3), 0310091-0310098. doi: 10.1115/1.3078301

Kweon, S., Beaudoin, A. J., & McDonald, R. J. (2010). Experimental characterization of damage processes in aluminum AA2024-O. *Journal of Engineering Materials and Technology, Transactions of the ASME, 132*(3). doi: 10.1115/1.4001445

Messner, M.C., Beaudoin A.J. & R.H. Dodds, Jr. (2014) Mesoscopic modeling of crack arrestor delamination in Al-Li: Primary crack shielding and T-stress effect", *International Journal of Fracture*, v. 188, pp. 229-249.

Messner, M.C., Beaudoin, A.J. & R.H. Dodds, Jr. (2015) An interface compatibility/equilibrium mechanism for delamination fracture in aluminum-lithium alloys , *Engineering Fracture Mechanics*, v 133, pp. 70-84.

Messner, M.C., Beaudoin, A.J. & R.H. Dodds, Jr. (2015), Consistent crystal plasticity kinematics and linearization for the implicit finite element method, Engineering Computations, v 32, pp. 1526-1548.

Mudrock, R.N., Lebyodkin, M.A., Kurath, P., Beaudoin, A.J. and T. A. Lebedkina (2011), "Strain-rate fluctuations during macroscopically uniform deformation of a solution-strengthened alloy , *Scripta Materialia, v* 65, pp. 1093–1096.

Riordan, T.E. (2007). Edge Cracking in the Hot Rolling of AA 5182. Thesis. University of Illinois at Urbana-Champaign.

There are no patents associated with the project.

The material model is implemented in the open-source code WARP3D http://www.warp3d.net/. WARP3D has been developed through support of many organizations over more that 15 years. PI Armand Beaudoin's contribution to the material model and documentation was supported by this DOE grant.

7. Model Description

The formulation of the mesoscale (crystal plasticity) model, as well as validation, is given in detail in the publication Messner, M.C., Beaudoin, A.J. & R.H. Dodds, Jr. (2015),"Consistent crystal plasticity kinematics and linearization for the implicit finite element method", Engineering Computations, v 32, pp. 1526-1548. Documentation for the model is also provided on the Warp3D website http://www.warp3d.net/.

Validation of Model using Tensile Test Data The work hardening response has been validated through deformation of a synthesized polycrystal. The polycrystal was adapted from the 'test74' example of Warp3d, and is thus part of the open-source distribution. A mesh of 5x5x5 grains, each discretized with 5x5x5 elements is subject to a tensile deformation. A comparison of the modeled stress-strain response is shown in Figure A.3. The mechanical threshold stress (MTS) material model implemented in WARP3D clearly captures the work hardening response for the AA 7050 material supplied by the Alcoa Technical Center.

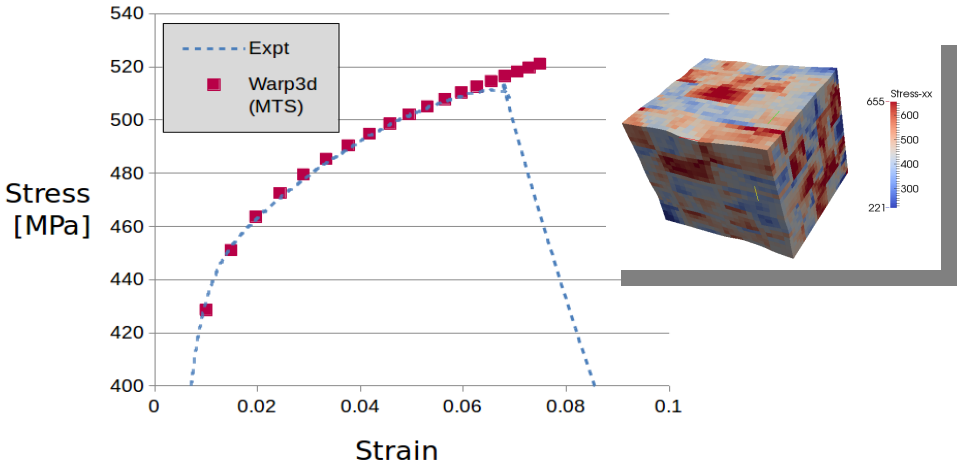

Figure A.3 – stress-strain response from Warp3d compared with data from tensile deformation of AA 7050. The synthesized polycrystal is shown to right of the figure.

The particular model for fracture developed through this project has a memory requirement of roughly 100Gb and runs well with 16 processors. The model has been run on a Linux workstation at UIUC and a Windows workstation at ATC.